HHS Public Access

Author manuscript

Sci Immunol. Author manuscript; available in PMC 2022 December 23.

Published in final edited form as:

Sci Immunol. 2021 October 15; 6(64): eabb6444. doi:10.1126/sciimmunol.abb6444.

Cholesterol 25-hydroxylase is a metabolic switch to constrain T cell-mediated inflammation in the skin

Hayato Takahashi[1,*], **Hisashi Nomura**[1], **Hisato Iriki**[1], **Akiko Kubo**[2], **Koichi Isami**[1], **Yohei Mikami**[3,12], **Miho Mukai**[1], **Takashi Sasaki**[4], **Jun Yamagami**[1], **Jun Kudoh**[5], **Hiromi Ito**[1], **Aki Kamata**[1], **Yutaka Kurebayashi**[6], **Hiroki Yoshida**[7], **Akihiko Yoshimura**[8], **Hong-Wei Sun**[9], **Makoto Suematsu**[2], **Jonh J. O'Shea**[3], **Yuka Kanno**[3], **Masayuki Amagai**[1,11]

[1]Department of Dermatology, Keio University School of Medicine, Tokyo 160-8582, Japan

[2]Department of Biochemistry, Keio University School of Medicine, Tokyo 160-8582, Japan

[3]Molecular Immunology and Inflammation Branch, National Institute of Arthritis and Musculoskeletal and Skin Diseases, National Institutes of Health, Bethesda MD 20892, USA

[4]Center for Supercentenarian Medical Research, Keio University School of Medicine, Tokyo 160-8582, Japan

[5]Laboratory of Gene Medicine, Keio University School of Medicine, Tokyo 160-8582, Japan

[6]Department of Pathology, Keio University School of Medicine, Tokyo 160-8582, Japan

[7]Division of Molecular and Cellular Immunoscience, Department of Biomolecular Sciences, Faculty of Medicine, Saga University, Saga 849-8501, Japan

[8]Department of Immunology and Microbiology, Keio University School of Medicine, Tokyo 160-8582, Japan

[9]Biodata Mining and Discovery Section, National Institute of Arthritis and Musculoskeletal and Skin Diseases, National Institutes of Health, Bethesda MD 20892, USA

[11]Laboratory for Skin Homeostasis, RIKEN Center for Integrative Medical Sciences, Kanagawa 230-0045, Japan

[12]Present address: Division of Gastroenterology and Hepatology, Department of Internal Medicine, Keio University School of Medicine, Tokyo 160-8582, Japan

Abstract

IL-27 is an immunoregulatory cytokine whose essential function is to limit immune responses. We found that the gene encoding cholesterol 25-hydroxylase (Ch25h) was induced in $CD4^+$ T cells by IL-27, enhanced by TGF-β, and antagonized by T-bet. Ch25h catalyzes cholesterol to generate 25-hydroxycholesterol (25OHC), which was subsequently released to the cellular

[*]**Correspondence:** Hayato Takahashi, MD, PhD, hayato_takahashi@keio.jp, Phone/Fax: +81-3-5363-3823/+81-3-3351-6880.

Author contributions: HT, HI, MM, KI, JY, and HI contributed to animal experiments and flow cytometry analysis. HN, AK, and AK contributed to *in vitro* analysis. YK contributed to the pathological analysis. YM, TS, JK, and HS contributed to data collection and analysis of RNA-seq. HT, AY, HY, MS, YK, JO, and MA contributed to overall project design. HT, YK, JO, and MA wrote the manuscript.

Competing Interests: HT and MA are inventors of a patent related to this work.

milieu, functioning as a modulator of T cell response. Extracellular 25OHC suppressed cholesterol biosynthesis in T cells, inhibited cell growth, and induced nutrient-deprivation cell death without releasing high-mobility group box-1. This growth inhibitory effect was specific to actively proliferating cells with high cholesterol demand and was reversed when extracellular cholesterol was replenished. Interestingly, Ch25h expressing $CD4^+$ T cells that received IL-27 and TGF-β signals became refractory to 25OHC-mediated growth inhibition *in vitro*. Nonetheless, IL-27 treated T cells negatively affected viability of bystander cells in a paracrine manner, but only if the bystander cells were in the early phases of activation. In mouse models of skin inflammation due to autoreactive T cells or chemically induced hypersensitivity, genetic deletion of *Ch25h* or *Il27ra* led to worsened outcomes. Thus, Ch25h is an immunoregulatory metabolic switch induced by IL-27 and dampens excess bystander T effector expansion in tissues through its metabolite derivative, 25OHC. This study reveals regulation of cholesterol metabolism as a modality for controlling tissue inflammation and thus represents a mechanism underlying T cell immunoregulatory functions.

One Sentence Summary:

Cholesterol 25-hydroxylase-expressing $CD4^+$ T cells limit pathogenic bystander T cell expansion by suppressing the cholesterol biosynthetic pathway with secreted 25-hydroxycholesterol.

INTRODUCTION

Helper $CD4^+$ T cells are crucial for proper host defense, but also contribute to the pathology of a wide variety of diseases. The lineage commitment of helper T subsets is initiated by cytokines in the microenvironment that activate transcriptomic programs for a particular subset while repressing other fates. The actions of proinflammatory cytokines such as interleukin (IL)-12, IL-4, and IL-6 are linked to inflammatory T helper subsets (Th1, Th2, and Th17), respectively, whereas those of IL-27 are more nuanced (1). IL-27 was originally reported to promote interferon (IFN)-γ production and T cell proliferation and considered as a proinflammatory cytokine (2, 3). However, the genetic deletion of IL-27 signaling predisposed mice to death due to unconstrained inflammation after *Toxoplasma gondii* and *Trypanosoma cruzi* infection, suggesting IL-27 plays an immunoregulatory role (4, 5). Subsequent studies have confirmed the regulatory roles of IL-27 in a series of infection, allergy, and autoimmune disease models (3, 6–8).

Several mechanisms underlying the immunoregulatory actions of IL-27 have been reported. The downregulation of master transcription factors such as GATA3 or RORγt (9, 10) during Th differentiation has been reported. Moreover, the induction of T-bet^+CXCR3^+ regulatory T cells (Tregs), a suppressive population specialized for Th1 inflammation, has been reported (11). These examples are relevant to specific circumstances but do not explain the broad regulatory effects of IL-27. Studies focusing on identifying downstream immunoregulatory molecules directly induced by IL-27 have suggested key molecules such as IL-10 (12, 13) and co-inhibitory receptors, including PD-1, activated protein C receptor, and podoplanin (14, 15) in T cells. However, these molecules are not exclusively induced by IL-27 (16–18), suggesting the involvement of other factors selective to IL-27 that contribute to drive IL-27 mediated immunoregulatory effect.

In this study, we sought to explore novel target molecules preferentially induced by IL-27 in helper T cells by referencing an IL-27-treated condition to other known lineages of effector or regulatory conditions (Th0, Th1, Th2, Th17, and iTreg). We identified cholesterol 25-hydroxylase (Ch25h) as an immunoregulatory molecule induced in cells treated with IL-27, and also by type I IFNs. Previous work has identified induction of Ch25h by type I IFNs in macrophages (19, 20). Critically though, IFN-γ does not efficiently induce Ch25h in T cells because T-bet acts as a negative regulator of Ch25h. In contrast, IL-27 effectively induces Ch25h and its product 25OHC. We provide evidence that alterations of cholesterol metabolism in cells receiving an IL-27 signal are crucial for regulating the viability of bystander lymphocytes in the early phase of active proliferation. We also show Ch25h-expressing T helper cells limit skin inflammation in a T cell-dependent autoimmune disease model.

RESULTS

Ch25h is selectively induced by IL-27 in CD4$^+$ T cells via STAT1

To identify potential target molecules relevant to the regulatory functions of IL-27, transcriptomic analysis was performed using *in vitro* differentiated CD4$^+$ helper subsets, including Th1, Th2, iTreg, Th17, and Th0, versus IL-27-treated CD4$^+$ T cells supplemented with transforming growth factor (TGF)-β, anti-IFN-γ, anti-IL-2, and anti-IL-4. The last condition was chosen to simulate IL-27-mediated regulatory conditions *in vitro* and maximize the likelihood of selecting for IL-27-induced events by antagonizing proinflammatory cytokine effects. Under these conditions, 146 genes were differentially expressed only in IL-27- and TGF-β-treated cells and not in the other subsets. Notably, *Ch25h*, which encodes cholesterol 25-hydroxylase, was the most differentially expressed gene (Table S1 and Fig. 1A). The specificity of *Ch25h* induction by IL-27 was further validated by individual pairwise comparisons with other subsets (Fig. S1). Real-time PCR confirmed that *Ch25h* was expressed at the highest levels in IL-27- and TGF-β-treated cells among other representative *in vitro* Th subsets (Fig. 1B).

Since a combination of IL-27 and TGF-β was used to identify *Ch25h*, the effect of each cytokine on *Ch25h* expression was evaluated separately. *Ch25h* expression was detected only in the IL-27-supplemented condition, but not with TGF-β, confirming the specificity of *Ch25h* induction by IL-27 (Fig. 1C). Next, the time course of *Ch25h* expression was recorded following IL-27 stimulation in CD4$^+$ T cells. *Ch25h* mRNA expression was detected on day 1, peaked on day 2, and declined on day 3 in CD4$^+$ T cells (Fig. 1D). Since IFNs have been shown to induce *Ch25h* expression in bone marrow-derived macrophages (BMDMs) (19, 20), the ability of IFNs and IL-27 to induce *Ch25h* in CD4$^+$ T cells was compared. Using quantitative PCR (qPCR), type I IFNs (IFN-α and IFN-β), but not IFN-γ, induced *Ch25h* with the range of doses tested. Nonetheless, IL-27 induced higher levels of *Ch25h* expression than type I IFNs (Fig. 1E). Immunocytostaining confirmed that IL-27 in combination with TGF-β upregulated Ch25h protein more than that with no cytokine control, and Ch25h protein was undetectable without stimulation (Fig. 1F). These results indicated that IL-27 and, to a lesser extent, type I IFNs are inducers of Ch25h production in CD4$^+$ T cells.

Next, our analysis was extended to examine whether *Ch25h* expression was observed in cells other than IL-27-treated naïve $CD4^+$ T cells with T-cell receptor (TCR) stimulation. Not only naïve $CD4^+$ cells but also memory $CD4^+$ T cells upregulated *Ch25h* when stimulated via TCR crosslinking with IL-27 (Fig. 1G). Conversely, *Ch25h* expression was not inducible in $CD8^+$ T cells, indicating that $CD4^+$ T cells preferentially induce Ch25h expression *in vitro* under IL-27-stimulating conditions (Fig. 1H).

Since IL-27 signaling is known to be mediated by the transcription factor Stat1, requirement of Stat1 for *Ch25h* induction in T cells was tested. Quantitative PCR revealed that IL-27-induced *Ch25h* expression was completely abolished in *Stat1*$^{-/-}$ $CD4^+$ T cells (Fig. 1I). This result is consistent with previous observations in BMDMs (19). These results indicate that $CD4^+$ T cells are selectively capable of expressing *Ch25h* in a Stat1-dependent manner under IL-27 stimulation.

T-bet negatively regulates Ch25h expression in $CD4^+$ T cells

STAT1 is also known to mediate IFN-γ signaling and both IL-27 and IFN-γ induce T-bet. Therefore, we speculated that IL-27-induced T-bet might also participate in *Ch25h* expression. In *Tbx21*$^{-/-}$ $CD4^+$ T cells, *Ch25h* was significantly upregulated compared with wild-type cells following IL-27 stimulation (Fig. 2A). Consistent with this result, *Tbx21*$^{-/-}$ T cells produced more 25OHC upon IL-27 stimulation than wild-type T cells (Fig. 2B). Interestingly, IFN-γ, which is the key cytokine to induce T-bet in Th1 cells (Fig. S2A), failed to induce *Ch25h* expression in wild-type T cells (Fig. 1E). However, in the absence of T-bet, this cytokine significantly upregulated *Ch25h* expression (Fig. 2A). These results indicate that T-bet is a negative regulator of *Ch25h* expression and subsequent 25OHC production.

To determine whether T-bet directly represses the transcription of *Ch25h*, we examined our previously published ChIP-seq data for histone marks and T-bet binding (21). Multiple enhancer marks (H3K4me1 and H3K27ac) were detected in wild-type cells downstream of the *Ch25h* locus and increased in intensity and number in *Tbx21*$^{-/-}$ cells (Fig. 2C). Furthermore, a subset of these enhancers was bound by T-bet (Fig. 2C), suggesting the direct involvement of T-bet in repressing *Ch25h* expression in wild-type cells.

When we tested the effect of TGF-β (0–20 ng/ml) in the presence of IL-27 (20 ng/ml), it was found that TGF-β enhanced *Ch25h* expression in a dose dependent manner (Fig. 2D: gray bars with WT cells) whereas the expression of T-bet was progressively suppressed (Fig. 2E). As T-bet was presumed to directly repress *Ch25h* expression (Fig. 2A and C), it was hypothesized that TGF-β might counter the effect of T-bet mediated repression of *Ch25h*. Indeed, in the absence of T-bet, *Ch25h* expression was always higher than wild-type T cells across all doses of TGF-β tested, and apparent dependency of *Ch25h* expression on TGF-β dosage disappeared in *Tbx21*$^{-/-}$ cells (Fig. 2D: white bars). These data indicate that the TGF-β-mediated enhancement of IL-27-induced *Ch25h* expression is likely mediated by the ability of TGF-β to downregulate T-bet expression (Fig. S2B).

Ch25h-expressing CD4$^+$ T cells produce 25OHC that down-regulates gene expression of cholesterol biosynthetic enzymes

Since *Ch25h* encodes the enzyme that converts cholesterol into 25-hydroxylcholesterol (25OHC) (22), IL-27-induced *Ch25h* expression was expected to induce production of intracellular 25OHC and possibly subsequent secretion of 25OHC into the culture medium. Gas chromatography-mass spectrometry (GC-MS) analysis showed that activated CD4$^+$ T cells produce little 25OHC, whereas IL-27 promoted a roughly seven-fold induction (Fig. 3A). Furthermore, the combination of IL-27 and TGF-β caused a massive increase in 25OHC production (Fig. 3B). In the absence of Ch25h, *Ch25h*$^{-/-}$ CD4$^+$ T cells were unable to produce 25OHC at all even when treated with IL-27 or IL-27, IFN-β and TGF-β combined, confirming an essential role of Ch25h for production of 25OHC (Fig. 3B).

Next, sequential measurement of 25OHC amounts in the culture supernatant was conducted over 5 days following IL-27 stimulation. Secreted 25OHC was first detected on day 2, peaked at approximately 100 nM on day 3, and was maintained until a gradual decrease occurred on day 5 (Fig. 3C). By contrast, *Ch25h* mRNA expression was notably diminished by day 3 (Fig. 1D). These results indicated that 25OHC is secreted within the first 2–3 days of IL-27 stimulation and remains present in the culture medium for at least another few days *in vitro*. These results showed that induction of *Ch25h* expression in CD4$^+$ T cells results in the production of 25OHC, which is released from T cells into their microenvironment following IL-27 signaling.

Next, the biological consequence of the presence of 25OHC in culture medium was evaluated by measuring the transcriptomic responses. CD4$^+$ T cells were treated with a range of concentrations of 25OHC (0, 10, 100, and 1000 nM) over time (days 1, 2, and 3). Depending on dosage, distinct biological pathways were impacted by 25OHC. With low doses of 25OHC, the biosynthesis of cholesterol and other metabolic pathways were affected (Fig. 3D: blue bars and Table S2). By contrast, with high doses, pathways related to the cell cycle, DNA replication, DNA repair, and centromeres were principally affected (Fig. 3D: orange bars and Table S3). The results pointed to metabolic pathways as a primary biological process impacted by 25OHC but as concentrations of this lipid increase, more profound influences on cell cycle and DNA replication pathways emerge.

Given these findings, we next focused our transcriptomic analysis on key enzymes and sterol-censoring molecules related to cholesterol biosynthesis (Fig. 3E, F and Fig. S3). As expected from pathway enrichment analysis, 25OHC down-regulated multiple cholesterol biosynthetic enzymes compared with other accessory components of the cholesterol pathway (Fig. 3E and Table S4, $p = 0.01$).

Previous studies have shown that 25OHC suppresses cholesterol biosynthesis by inhibiting the transport of sterol regulatory element-binding protein (SREBP) and SREBP cleavage-activating protein (SCAP) complex to the Golgi. Translocation of SCAP-SREBP from the endoplasmic reticulum to the Golgi is the critical initial step for the cleavage and activation of SREBP as a transcription factor to initiate cholesterol synthesis and uptake (23). In line with previous findings (24), our computational analysis revealed that significant enrichment of SREBP1 and SREBP2-binding DNA motifs was associated with genes

depicted as 25OHC-down-regulated genes that belong to the cholesterol biosynthesis pathway (Fig. 3G). Based on these results, it seems plausible that exposure to 25OHC limits activation of transcription factor SREBP. Insufficient availability of SREBP, in turn, leads to downregulation of key metabolic enzymes required for cholesterol biosynthesis, leading to suppression of *de novo* cholesterol biosynthesis.

25OHC impairs cell proliferation and induces cholesterol-deprived cell death

Since IL-27-stimulated T cells were identified as a source of 25OHC, we next sort to determine how secreted 25OHC might influence the cellular phenotype of the surrounding T cells via suppressing cholesterol synthesis. According to previous reports, 25OHC mediated suppression of sterol synthesis, abolished DNA synthesis and lymphocyte proliferation (25–28). 25OHC was exogenously added to the *in vitro* culture of T cells stimulated with TCR, and cell division was measured by carboxyfluorescein diacetate succinimidyl ester (CFSE) labeling. Among the doses of 25OHC tested, cell proliferation was significantly suppressed at 100 nM, and almost completely abrogated at 1000 nM (Fig. 4A), in line with previous reports (26–28). When cell viability was evaluated by a combination of 7-aminoactinomycin D (7-ADD) staining and cell size (FSC), impaired viability was observed in a dose-dependent manner (Fig. 4B). The effect of 25OHC on cell size became evident at approximately 100 nM (Fig. 4C) and resulted in a decreased frequency of 7-ADD negative live cells (Fig. 4D). The effect of 25OHC on cell viability was present at 24 h of cell culture, and became more evident at later time points (Fig. 4E and Fig. S4A). In the absence of TCR- or IL-2-dependent activation, T cells were resistant to the effect of 25OHC even at the highest concentration tested (Fig. S4A; Fig. 4C, D). Taken together, these results suggested that 25OHC impairs cell proliferation and viability depending on the metabolic demands of T cells, i.e. whether cells receive activation signals such as antigen stimulation or IL-2.

Given that cells with high metabolic demands are susceptible to 25OHC and prone to cell death, we next asked if the 25OHC-stressed cells could perpetuate the inflammatory response further by releasing danger signals such as alarmins. High mobility group box-1 (HMGB-1) is released to extracellular space from necrotic cells, but no HMGB-1 was produced by 25OHC-treated cells (Fig. S4B) indicating that this mode of cell death by 25OHC was not associated with alarmin release.

As 25OHC is further metabolized to 7α,25-dihydroxycholesterol (7α,25OHC) by Cyp7b1 (Fig. 4F), the question arose whether a downstream metabolite of 25OHC could also confer similar inhibitory effects as 25OHC. It was found that 25OHC, but not 7α,25OHC, induced cell death of $CD4^+$ T cells (Fig. 4G). Moreover, $CD8^+$ T cells were also susceptible to cell death by 25OHC in a dose-dependent manner (Fig. S4C). Therefore, 25OHC, but not 7α,25OHC, could render $CD4^+$ and $CD8^+$ T cell populations vulnerable to cell death.

Given that insufficient cholesterol supply is likely a mechanism underlying cell death induced by 25OHC, a rescue experiment was conducted by providing an exogenous source of cholesterol in the culture media in addition to 25OHC. We found that addition of cyclodextrin–cholesterol efficiently rescued cell viability at low to medium doses of 25OHC; although, prevention of cell death was limited at higher doses of 25OHC (Fig. 4H, I). This finding was consistent with our transcriptomic analysis (Table S3) indicating that pathways

related to the cell cycle or DNA repair were critically impacted at high concentrations of 25OHC, such that the restoration of intracellular cholesterol levels alone did not fully rescue cells exposed to high doses of 25OHC (Fig. 4H, I). These results collectively indicated that 25OHC-induced cell death is in part attributable to the reduction in intracellular cholesterol owing to the impaired *de novo* biosynthesis in activated T cells with high metabolic demands.

Ch25h-expressing CD4$^+$ T cells impair viability of bystander T cells at early stage of TCR activation in a paracrine manner

Our findings so far collectively connect IL-27 (cytokine) to Ch25h (enzyme) to 25OHC (metabolite) as a series of molecular events leading to impaired supply of cholesterol for avidly proliferating T cells with high metabolic demands. As Ch25h-expressing cells produce and release 25OHC into culture medium (Fig. 3A–C), we considered the possibility that Ch25h-expressing WT cells might be negatively impacted by autocrine 25OHC during the course of IL-27 exposure. By contrast, we expected that *Ch25h*$^{-/-}$ CD4$^+$ T cells might have growth advantage due to lack of autocrine 25OHC production. Contrary to our expectations, there was no significant difference in cell viability and proliferative activity between WT and *Ch25h*$^{-/-}$ CD4$^+$ T cells cultured separately but in the same IL-27 included conditions (Fig. S5). These results indicated that Ch25h-expressing cells are refractory to growth inhibitory effect of autocrine 25OHC.

This unexpected finding led us to consider that the timing of cell activation and 25OHC exposure was relevant in terms of inhibition of cell growth and viability. Normally, secretion of 25OHC required two days following activation of CD4$^+$ T cells (TCR crosslinking plus IL-27 and TGF-β; Fig. 3C). To clarify the sensitivity of activated T cells, we added exogenous 25OHC (200 nM) to *in vitro* T cell cultures at different time points. The inhibitory effect of 25OHC on cell viability was most evident if 25OHC was present concomitant with cell activation but was reduced if 25OHC addition was delayed. In fact, 25OHC had no effect if added 48 or 72 hours after activation (Fig. 5A). These results indicated that because 25OHC production is delayed in IL-27/ TGF-β activated cells, the cells are largely protected from inhibitory action of autocrine 25OHC. However, T cells in early phase of TCR-mediated activation (<48 hrs) are susceptible to 25OHC-mediated impairment on cell viability.

Given the timing of 25OHC production and the refractoriness of activated cells, the possibility of paracrine versus autocrine effects of 25OHC on bystander cells seemed more likely. To test this, sequential *in vitro* cultures were performed as described in Fig. 5B. First, WT or *Ch25h*$^{-/-}$ naïve CD4$^+$ T cells were activated with TCR crosslinking in the presence of IL-27+TGF-β for 2 days to generate effector cells. After removing effector cells, CFSE-labelled *Il27ra*$^{-/-}$ cells were introduced as responder cells to the pre-conditioned media and the cells were cultured for another 3 days. During the second culture, TGF-β neutralizing antibody was added to make certain that the responder cells did not receive IL-27 signaling (due to the lack of receptor) or TGF-β (due to neutralization) to induce autocrine Ch25h production. In this experimental setting, Ch25h-expressing WT effector cells impaired the viability and proliferation of responder cells, indicative of a paracrine effect (Fig. 5C). As

a control, IL-27+TGF-β-treated *Ch25h*$^{-/-}$ T cells (1st culture) had no effect on bystander cells (2nd culture), thus linking IL-27/TGF-β mediated induction of Ch25h and 25OHC production. These results collectively indicate that Ch25h-expressing CD4^{+} T cells impaired viability and proliferation of bystander cells at early stages of activation in a paracrine manner.

Ch25h expressed in T cells is important to restrain tissue inflammation in experimental autoimmune dermatitis

Our *in vitro* results point to the generation of Ch25h-expressing T cells that result from IL-27 signal to influence bystander cells during heterogenous T effector responses. To determine whether this regulatory axis of IL-27-Ch25h-25OHC is relevant *in vivo*, a T cell-mediated autoimmune model of skin disease termed experimental autoimmune dermatitis (EAD) was used (29). In this model, *Rag2*$^{-/-}$ mice were adoptively transferred with desmoglein 3 (Dsg3)-specific TCR transgenic CD4^{+} T cells (H1 T cells), which expand in lymphopenic host, then infiltrate to the skin and attack Dsg3-bearing epidermal keratinocytes leading to interface dermatitis (ID). Several Th effector subsets including Th1, Th17 and others are identified during skin inflammation, among which IFN-γ is indispensable for inducing pathological changes (29). The relevance of IL-27-dependent 25OHC production on the extent of inflammation was evaluated by transferring WT versus *Il27ra*$^{-/-}$-H1 T cells. The *Rag2*$^{-/-}$ recipient mice receiving *Il27ra*$^{-/-}$-H1 T cells showed significantly greater clinical inflammation scores than WT H1 T cells (Fig. 6A), with severe epidermal damage associated with increased degenerative keratinocytes (Fig. 6B: red arrows). As expected, the mice that received WT H1 T cells induced mRNA expression of *IL-27p28* in dendritic cells isolated from the inflamed skin and from skin-draining LNs (Fig. S6A). These results collectively demonstrated that IL-27 signaling plays a key role in constraining skin inflammation in EAD.

Next, involvement of IL-27-Ch25h axis in regulating autoreactive T cells was evaluated in EAD. Expression of *Ch25h* was observed in H1 T cells isolated from the inflamed skin, but not in skin-draining LNs, indicating the localized expression of *Ch25h*, limited to the site of inflammation (Fig. S6B). This upregulation of *Ch25h* was significantly reduced in T cells unable to respond to IL-27 (*Il27ra*$^{-/-}$-H1 T cells) during inflammation (Fig. S6C).

We confirmed these results using an alternative *in vivo* immunization model that did not require adoptive transfer of transgenic T cells. WT, H1 transgenic or *Il27ra*$^{-/-}$-H1 mice were immunized by Dsg3 peptide and T helper effector cells (CD4^{+}CD62L^{low}CD44^{hi}) were sorted after 1 week of immunization and subjected to qPCR analysis for *Ch25h* mRNA expression. Compared with WT, H1 mouse expressed higher levels of *Ch25h* mRNA in activated effector T cells isolated from skin but not lymph nodes (Fig. S6D), and the induction of Ch25h mRNA was abrogated in *Il27ra*$^{-/-}$-H1 mice (Fig. S6E). These results indicated that IL-27-dependent induction of Ch25h in T helper cells *in vivo* during the course of skin autoimmunity either generated by peptide immunization or adoptive T cell transfer.

For further confirmation of our model, *Ch25h*$^{-/-}$ mice were crossed with H1 tg mice. Transfer of *Ch25h*$^{-/-}$-H1 T cells resulted in significantly greater skin inflammation

compared to transfer of WT H1 T cells (Fig. 6C, D). Histological examination revealed prominent tissue inflammation (Fig. 6E) and increased number of autoreactive TCRVβ$^+$ CD4$^+$ T cells in the recipients of *Ch25h*$^{-/-}$-H1 T cells (Fig. 6F: red cells). Furthermore, the number of H1 T cells in the inflamed tissue was significantly higher in the absence of Ch25h (Fig. 6G). When percentages of H1 T cell fractions were measured, the impact of *Ch25h* deficiency to expand H1 T cells was evident only in the skin but not in secondary lymphoid organs (Fig. 6H), indicating its functional relevance limited at the site of inflammation. These results indicated that Ch25h, induced in CD4$^+$ T cells via IL-27, is a key enzyme that limits the extent of skin inflammation by constraining the expansion of pathogenic cells in the lesional skin, most likely through secretion of 25OHC in the inflamed tissue.

Loss of Ch25h exacerbates skin contact hypersensitivity

Finally, to broaden the relevance of Ch25h in controlling skin inflammation, we employed a contact hypersensitivity model in which IL-27 is known to play a critical role (30). After sensitization in the abdominal skin with 1-fluoro-2,4-dinitrobenzene (DNFB), contact hypersensitivity reaction was assessed by ear thickness in WT and *Ch25h*$^{-/-}$ mice following topical DNFB application. The kinetics of skin inflammation differed between the two mice, with prolonged inflammation being observed in *Ch25h*$^{-/-}$ mice (Fig. 7A, B). Histological examination of inflamed skin showed enhanced inflammation in *Ch25h*$^{-/-}$ mice (Fig. 7C). Importantly, exogenous administration of 25OHC via intraperitoneal injection reversed the severity of skin inflammation, confirming that Ch25h-25OHC axis is relevant to constrain the degree of skin inflammation in the model of DNFB-induced contact hypersensitivity (Fig. 7D, E).

DISCUSSION

Cholesterol and its derivatives are essential for maintaining cellular functions in broad range of cells. In immune cells, cholesterol and its derivatives are reported to have anti-viral, inflammatory, and anti-inflammatory properties, but also have roles in immune cell guidance involving innate and adaptive cells (31–36). In this study, we showed that CD4$^+$ T cells have the potential to produce Ch25h, a cholesterol-metabolizing enzyme, and to secrete the metabolite, 25OHC, to the cellular milieu in response to IL-27. Extracellular 25OHC impaired the viability and proliferation of TCR/IL-2 stimulated T cells by impeding cellular cholesterol biosynthesis while metabolically quiescent naïve cells were spared from 25OHC-mediated inhibition (Fig.S4A). Importantly, 25OHC-mediated inhibition was effective only in a narrow window of early T cell activation (<48 hrs) and the T cells expressing Ch25h and secreting 25OHC are themselves refractory to this metabolite. This is because activated T cells apparently have passed a vulnerable window of 48 hrs after which they then produce 25OHC (Fig.3C). Instead, Ch25h-expressing T cells can mediate a paracrine regulatory role via 25OHC production to suppress other cells, including bystander T cells. This effect can be demonstrable in terms of reduced bystander T cell proliferation *in vitro*, but only if the bystander cells are in the early phase of TCR-dependent activation. In contract, the cells that have proliferated for more than 2 days, most likely regardless of polarizing cytokine conditions, become refractory to 25OHC (Fig.5A).

Expression of Ch25h and production of 25OHC has been described as having diverse but critical effects in immune cells.(19, 37). For example, 25OHC activates the integrated stress response, which may contribute to its antiviral activity (38). Ch25h and 25OHC inhibit viral entry and replication in several cell lines (19, 20, 39), and render host cells resistant to cholesterol-dependent cytolysin-induced pore formation during bacterial infection (40). Notably, the effect of 25OHC to block SARS-Cov-2 replication has been reported (41). Also Ch25h/25OHC suppress immunoglobulin class switching to IgA in B cells (42). On the other hand, the deficiency of *Ch25h* results in the overproduction of IL-1 from macrophages, indicating 25OHC inhibits IL-1 (34, 43). Accordingly, *Ch25h*-deficient mice exhibit increased sensitivity to septic shock and exacerbated experimental autoimmune encephalomyelitis (EAE), because 25OHC limits AIM2-dependent inflammasome activation by regulating cholesterol synthesis and mitochondrial DNA release (43, 44). Taken together, our findings reinforce the idea that the Ch25h–25OHC axis supports immunoregulatory function across broader immune cell populations including T cells. While our adoptive T cell transfer model point to the impact of T cell specific 25OHC production, the caveat of interpreting effector T cell function in immunodeficient host needs to be considered.

On the other hand, there is no doubt that the role of Ch25h is rather complex and context dependent (i.e., dosage, cell type, disease model), and seemingly contradictory findings have been reported. For example, 25OHC amplifies expression of genes encoding inflammatory cytokines including *Il6*, *Il8* and Csf1 (45). Also 25OHC plays a proinflammatory role by suppressing type 1 regulatory T (Tr1) cells (46). 25OHC suppresses both proliferation of Tr1 cells as well as production of IL-10, leading to the proposal of a proinflammatory role of Ch25h/25OHC as a result of suppressing suppressor cells. What was not evaluated in the report is the effect of 25OHC on T effector cells, and *in vivo* outcome of 25OHC effect on inflammation, which is determined by balancing action of effector vs regulatory cell subsets. In this regard, we found that 25OHC impacted cell proliferation and viability of freshly activated effector cells with high metabolic demand. Using two distinct skin inflammation models *in vivo*, we found that the lack of Ch25h resulted in more severe and more prolonged inflammation, indicating a regulatory role of Ch25h-25OHC axis *in vivo*. Based on our *in vitro* result, we envision that Ch25h25-OHC axis has the potential of exerting a regulatory role in a paracrine manner *in vivo* as well. Although we are unable to pinpoint the precise cells that produce and respond to 25OHC in our *vivo* models, the emergence of $Ch25h^{+}$ T cells responding to IL-27 could be one of such 25OHC producers. This mechanism could shape tissue microenvironment during a resolution phase in which further expansion of newly activated T cells and other inflammatory immune cells are constrained.

The molecular mechanisms underlying 25OHC-induced cell death and signals converging to regulate this process are intricate. An interesting observation in our study is the anti-IL-2 antibody-mediated rescue of cell death. Anti-IL-2 antibody restored cell death even at high concentrations of 25OHC, whereas exogenously added cyclodextrin–cholesterol could not save the cells. Removal of IL-2 signaling resulted in slowed cell growth, and the reduction in the proliferative state effectively saved cells from cell death otherwise caused by 25OHC *in vitro*. Our pathway analysis of 25OHC-treated cells also revealed the cell cycle, DNA repair, and centromeres as the biological processes affected by high concentrations of 25OHC in line with previous reports describing suppressive effect of 25OHC on activated lymphocyte

proliferation (26–28). Since notable concentrations of 25OHC (~ 300 nM) were detected in the serum of mice administered the TLR4 agonist (42), it is reasonable to believe that states of immune cell activation and proliferation, rather than effector phenotypes such as Th1 and Th17 e.g., are key factors that determine whether a particular subset of immune cells is or is not affected by 25OHC. Indeed, local administration of 25OHC to lung modulated inflammation induced by asthma or injury (47).

The importance of cholesterol regulation is considerably evident in activated T cells because the demand for essential nutrients, including cholesterol, is very high. T cells reprogram their metabolism by simultaneously inducing SREBP2 and repressing liver X receptor signaling, with progression into the cell cycle sustained by SREBP2 activation and cholesterol biosynthesis (48–50). Conversely, the down-modulation of cholesterol biosynthesis compromises cell cycle progression and metabolic reprogramming of activated T cells (26–28). The induction of *Ch25h* and production of 25OHC by IL-27 and TGF-β represent another aspect of cholesterol metabolism, which does not impede non-proliferating resting T cells that do not contribute to pathogenic immune responses. Instead, 25OHC-mediated suppression of cell proliferation and induction of cell death likely contribute to the effective removal of highly active pathogenic cells from inflamed tissues in the resolution phase without affecting other quiescent resident cells. In this regard, it is also interesting to note that in our T cell transfer dermatitis model, IL-27 appears to be expressed as much in draining LN DC as in skin DC, yet dermatitis-invoking H1 T cells only upregulated Ch25h in the skin. It is tempting to speculate that the combination of strong TCR engagement at the site of inflammation in conjunction with the availability of TGF-β in the skin might favor local induction of Ch25h by IL-27.

The cell state selective action of 25OHC raises the intriguing possibility of pharmacologically modifying cholesterol synthesis to control autoimmune or inflammatory diseases. Recently, cholesterol and other cellular metabolites have emerged as promising new targets to modulate immune responses (48). For example, pharmacological blocking of cholesterol esterification in tumor-infiltrating lymphocytes altered intracellular cholesterol distribution to boost the amount of cholesterol in the plasma membrane. This resulted in enhanced tumor immunity owing to enhanced TCR clustering and immunological synapse formation (51). By contrast, our study suggested a way to constrain the immune response via Ch25h and 25OHC, which suppresses cell-intrinsic cholesterol synthesis. Unlike many available immunosuppressants that indiscriminately suppress all immune cells, designing a compound that mimics or induces 25OHC could selectively target proliferating pathogenic cells in autoimmune conditions. In this manner, the adverse effects encountered previously could be minimized while delivering targeted anti-inflammatory control.

MATERIALS AND METHODS

Mice

C57BL/6J mice were purchased from Sankyo Labo Service Corporation (Tokyo, Japan). *Tbx21*$^{-/-}$ mice (52) and *Stat1*$^{-/-}$ mice (53) were provided by Dr. Akihiko Yoshimura; *Il27ra*$^{-/-}$ mice (3) were provided by Dr. Hiroki Yoshida; *Ch25h*$^{-/-}$ mice were purchased from the Jackson Laboratory (Bar Harbor, ME, USA). *Rag2*$^{-/-}$ mice were purchased from

the Central Institute for Experimental Animals (Kanagawa, Japan). Dsg3H1 mice were generated as previously reported (29). The Keio University Institutional Animal Care and Use Committee approved all the experiments.

Reagents

Cholesterol, 25OHC, and 7α,25OHC were purchased from Sigma-Aldrich (St. Louis, MI, USA) or Avanti Polar Lipids (Alabaster, AL, USA), resolved in DMSO, and stored at −80°C until use. Hexane, ethylacetate, and sodium sulfate anhydrous were purchased from Nacalai Tesque (Kyoto, Japan). 25-hydroxycholesterol and D6-25-hydroxycholesterol were obtained from Avanti Polar Lipids. Cholesterol-methyl-β-cyclodextrin was purchased from Sigma-Aldrich.

Cell culture

Cell culture was performed in RPMI supplemented with 10% fetal bovine serum, 2 mM glutamine, 100 IU/ml penicillin, 0.1 mg/ml streptomycin, 1 mM sodium pyruvate, and 2.5 μM β-mercaptoethanol. Naïve $CD4^+$ T cells ($CD4^+CD62L^{hi}CD44^{lo}CD25^-$ cells), memory $CD4^+$ T cells ($CD4^+CD62L^{lo}CD44^{hi}CD25^-$ cells), naïve $CD8^+$ T cells ($CD8^+CD62L^{hi}CD44^{lo}CD25^-$ cells), and memory $CD8^+$ T cells ($CD8^+CD62L^{lo}CD44^{hi}CD25^-$ cells) were isolated using a MoFlo XDP cell sorter (Beckman Coulter, Brea, CA, USA) or FACS Aria II (BD Biosciences, San Jose, CA, USA) and cultured in plate-bound anti-CD3 and anti-CD28 (10 μg/ml each) in combination with 20 ng/ml IL-12 and 10 μg/ml anti-IL-4 (11B.11; NCI Frederick, Frederick, MD, USA) for Th1; 20 ng/ml IL-4 and 10 μg/ml anti-IFN-γ (XMG1.2; Bio X Cell, Lebanon, NH, USA) for Th2; 2 ng/ml TGF-β, 20 ng/ml IL-6, anti-IFN-γ, and 10 μg/ml anti-IL-2 (S4B6, BD Biosciences) for Th17 (TGF-β); 20 ng/ml IL-1β, 20 ng/ml IL-6, 50 ng/ml IL-23, anti-IFN-γ, anti-IL-2, 5 μg/ml anti-TGF-β1 (R&D Systems, Minneapolis, MN, USA), and 5 μg/ml anti-TGF-β2/1.2 (R&D Systems) for Th17 (IL-23); 20 ng/ml TGF-β, 50 U/ml IL-2, and anti-IFN-γ for iTreg; anti-IFN-γ and anti-IL-2 for Th0, for 3 days. IFN-β, IFN-α, and IL-27 were used in combination with anti-CD3 and anti-CD28 antibody stimulation for 2 days unless indicated for Ch25h induction. Cytokines were purchased from R&D Systems. For some experiments, $CD8^+$ cells were isolated using magnetic beads (Miltenyi Biotec, Bergisch Gladback, Germany) and stimulated with anti-CD3 and anti-CD28 as mentioned above. The effect of Ch25h on $CD4^+$ T cells was determined by culturing naïve $CD4^+$ T cells in plate-bound anti-CD3 and anti-CD28 (3 μg/ml each) in combination with various concentrations of 25OHC (Sigma-Aldrich). In some experiments, IL-2 was neutralized using anti-IL-2 antibody (S4B6). Cell viability and HMGB-1 release were assessed using a flow cytometer and HMGB-1 Detection Kit (Chondrex, Redmond, WA, USA), respectively.

Experiments with conditioned culture medium

Conditioned culture medium was prepared by culturing naïve WT and *Ch25h*$^{-/-}$ $CD4^+$ T cells with IL-27 (20 ng/ml) and TGF-β (20 ng/ml) along with anti-CD3 and CD28 antibodies for two days. The supernatant was collected after centrifugation and used for the 2nd *in vitro* culture of 3 days using *Il27ra*$^{-/-}$ $CD4^+$ responder T cells that were labelled with carboxyfluorescein diacetate succinimidyl ester (CFSE, ThermoFisher). To block TGF-β

signals, neutralizing anti-TGF-β1 and TGF-β2 antibodies (2 μg/ml for each, R&D) were also added. %Divided was calculated by FlowJo (BD).

Transcriptome analysis in Th subsets

Total RNA was prepared from 1 million cells using the mirVana miRNA Isolation Kit (Thermo Fisher Scientific). Subsequently, 1 μg of total RNA was used to prepare the RNA-seq library using the TruSeq SRRNA Sample Prep Kit (Illumina, San Diego, CA, USA), according to the manufacturer's instructions. The libraries were sequenced for 50 cycles (single read) using the Hiseq 2000 (Illumina). Sequence reads from each cDNA library were mapped onto the mouse genome (build mm9) using tophat 2.0.3. The obtained data were used to calculate gene expression values normalized based on fragment per kilobase exon model per million mapped reads using Cufflinks 1.3.0. Transcripts with normalized values of more than 1 were considered to be expressed in cells. RNA-seq data for naïve CD4 T cells previously deposited in GEO (GSE45975) were used in Figure 1A.

Transcriptome analysis: 25OHC-affected genes

Naïve $CD4^+$ T cells were treated with different concentrations of 25OHC (0, 10, 100, and 1000 nM). After 1, 2, or 3 days of 25OHC treatment, cells were collected, and total RNA was isolated using the RNeasy Mini Kit (Qiagen), according to the manufacturer's instructions. The quality of extracted RNA was evaluated using the RNA integrity number and Agilent 2100 Bioanalyzer (Agilent Technologies, Santa Clara, CA, USA). The DNA libraries for mRNA-seq were constructed using the SureSelect Strand-Specific RNA Library Prep Kit (Agilent Technologies), according to the manufacturer's instructions, and sequenced using HiSeq 2500 (Illumina). The DNA sequence was trimmed using the trim galore program (version 0.4.4; http://www.bioinformatics.babraham.ac.uk/projects/trim_galore/) with the cutadapt program (version 1.14), and the trimmed sequence was mapped to the mouse genome (mm9) using STAR (version 020201). The number of reads of each gene was calculated using featureCounts (version 1.6.2) with the mm9 annotation [version July 17, 2015 (UCSC)]. The mapped read data were normalized using rlog methods in the Deseq2 R package (version 1.16.1). Multivariate analysis for differential expression was performed using Deseq2 with variable 25OHC concentrations and culture days. Finally, genes that showed significant differences ($p < 0.01$; log2 fold change, ≥ 1 or ≤ -1) by multivariate analysis were analyzed using DAVID (version 6.8; https://david.ncifcrf.gov) with default conditions to detect the candidate pathways associated with these genes. In the analyses, normalized read counts of genes associated with the sterol biosynthetic process (GO ID:0016126) in 25OHC-treated $CD4^+$ T cells on day 1 were expressed as a heatmap. Genes not expressed in $CD4^+$ T cells were excluded from the analysis. The calculated value from non-treated cells was defined as 1. Enrichment analyses of transcription factor-binding DNA motifs were performed with CiiiDER (L. J. Gearing et. al. *PLoS One* **14**, e0215495 (2019)).

RT-PCR

Total RNA was isolated using the RNeasy Mini Kit (Qiagen, Hilden, Germany) in combination with RNase-free DNase. cDNA synthesis was performed using TaqMan

Reverse Transcription Reagents (Applied Biosystems, Foster City, CA, USA). Quantitative PCR was performed using StepOnePlus Real-Time PCR System (Applied Biosystems) with Universal SYBR Select Master Mix using the following primers: Ch25h forward: 5′-GCGACGCTACAA GATCCA-3′, Ch25h reverse: 5′-CACGAACACCAGGTGCTG-3′, β-actin forward: 5′-CGATGCCCTGAGGCTCTTT-3′, β-actin reverse: 5′-TGGATGCCACAGGATTCCA-3′, Tbx-21 forward: 5′-CGTGGAGGTGAATGATGGA-3′, and Tbx-21 reverse: 5′-TGAGTGATCTCTGCGTTCTGGTA-3′, IL-27p28 forward: 5′-TGTCCACAGCTTTGCTGAAT-3′, IL-27p28 reverse: 5′-AAGGGCCGAAGTGTGGTAG-3′. In some experiments, *Ch25h* expression was quantified with TaqMan probe commercially available. All gene expressions were normalized by β-actin expression and shown as relative expression levels.

Flow cytometry

A single-cell suspension of spleen, skin-draining LNs, mesenteric LNs, and skin was appropriately stained using 7-aminoactinomycin D, anti-Vβ6 chain-BV421 (RR4-7), anti-CD8α-PE/Cy7 (53–6.7), anti-CD25-PE (PC61), anti-CD44-FITC (IM7), anti-CD62L-APC (MEL-14), and anti-CD4-APC/Cy7 (RM4-5). The data were collected by FACSCanto II (BD) and analyzed by FlowJo (BD).

Sample preparation for GC-MS

To 1 ml of culture medium, 4 ml of *n*-hexane containing deuterium-labeled internal standards (1 μg D6-25OHC) was added and mixed using a vortex mixer. Sterols were extracted with an additional 4 ml of *n*-hexane. Following dehydration with sodium sulfate, organic fractions were applied on Sep-Pak Silica cartridges (WAT023595; Waters, Mississauga, Ontario, Canada) and eluted with 1.5 ml of ethyl acetate. The eluents were dried under a nitrogen stream. The residue was dissolved in 10 μl of pyridine and 50 μl of BSTFA + TMCS (99:1; #33148; Supelco Inc., St. Louis, MO, USA) for trimethylsilylation. The derivatization reaction was performed for 30 min at 40°C.

GC-MS analyses

GC-MS analysis was performed on a Shimadzu GC-MS QP2010 Ultra equipped with an AOC20i autoinjector and Rtx-5MS column (30 m × 0.25 mm × 0.25 μm df) in the 70 eV electron ionization mode. The oven temperature program was as follows: 60°C for 3 min and 15°C/min to 330°C, where the temperature was maintained for 10 min. The carrier gas was helium with a constant flow speed of 39.0 cm/s. One microliter was injected in the 10:1 split ratio with an injector temperature of 250°C; the MS interface temperature was held at 280°C. Selected ion monitoring for quantification was performed by recording the ions at *m/z* 456.40 for the 25-hydroxycholesterol-trimethylsilyl derivative and at *m/z* 462.40 for D6-25-hydroxycholesterol.

Experimental autoimmune dermatitis

$CD4^+V\beta6^+CD25^-CD62L^{hi}CD44^{lo}$ Dsg3-specific TCR transgenic naïve T cells were isolated from Dsg3H1 and *Ch25h*$^{-/-}$Dsg3H1 mice and adoptively transferred (0.5 to 3 × 10^5 cells/head) into *Rag2*$^{-/-}$ mice with $B220^+$ B cells (2 to 6 × 10^5 cells/head)

derived from rDsg3-immunized *K5-Dsg1tg-Dsg3*$^{-/-}$ mice (54). In some experiments, TCR transgenic naïve T cells were obtained from *Il27ra*$^{-/-}$Dsg3H1 mice. The clinical severity of skin phenotype was evaluated at indicated time points according to the scoring system (Table S5). For qPCR, CD11c^{+} DCs, and Dsg3-specific CD4^{+}Vβ6^{+} T cells were isolated by FACSAriaIII (BD). Dsg3H1 mice were immunized with 1 μg Dsg3 peptide, RNKAEFHQSVISQYR, with CFA (Sigma-Aldrich) as an adjuvant.

Contact hypersensitivity model

To induce contact hypersensitivity (CHS) responses, 25 μL of 0.5% 1-fluoro-2,4-dinitrobenzene (DNFB; Nacalai Tesque, Kyoto, Japan) dissolved in acetone/olive oil (4:1) was applied (for sensitization) to the shaved abdomens of mice (sensitization), which were challenged with 20 μL of 0.15% DNFB (applied to the ear) 5 days later. Changes in ear thickness were measured at specific subsequent time points by using a thickness gauge (Teclock PG-20, Nagano, Japan). In some experiments, 1 μmol 25OHC or vehicle (DMSO diluted 30 folds with PBS) were intraperitoneally injected in mice once a day for five days after sensitization. Graphs of ear thickness was plotted along the time points for vehicle control vs 25OHC treatment, and area under the curve was calculated for each and the difference was statistically evaluated by t-test using GraphPad Prism (GraphPad Software, San Diego, California, USA). The difference in ear thickness between experimental groups were evaluated by two-way ANOVA.

Pathological and immunofluorescence analysis

The palate, esophagus, and skin of *Rag2*$^{-/-}$ mice with the experimental autoimmune dermatitis phenotype or CHS responses were fixed in 10% formalin and stained with hematoxylin and eosin. Sections were observed under a DMD108 microscope (Leica, Wetzlar, Germany). For immunofluorescence staining, 10 μm cryosections of the palate were fixed with paraformaldehyde and stained with anti-CD4 and DAPI. Sections were observed under a fluorescence microscope (Axio Observer.Z1; Carl Zeiss, Oberkochen, Germany). Briefly, for Ch25h staining, differentiated T cells were spun onto microscope slides using a cytospin apparatus and fixed with acetone. Sections were stained with rat anti-Ch25h monoclonal antibody (185-1; BML) and stained with Alexa488-conjugated goat anti-rat IgG antibody, Alexa647-conjugated anti-CD4 antibody (RM4-5), and DAPI.

Statistics

All data are shown as mean ± SEM of triplicate assays and analyzed by Student's *t*-test using GraphPad Prism (GraphPad Software, San Diego, California, USA) unless otherwise specified.

Supplementary Material

Refer to Web version on PubMed Central for supplementary material.

Acknowledgments:

We thank Mr. Jim Simone (NIAMS, NIH) and Mr. Akira Sonoda (Core Instrumentation Facility, Keio University) for cell sorting; Dr. Naotomo Kambe (Kyoto University) for valuable discussion; and Ms. Mie Furuhashi (Keio University) for technical support.

Funding:

This research was supported by AMED (grant numbers JP18gm5910015, JP15lm0103010j0002, JP18gm1210001h0001 and JP21gm1110009), JSPS KAKENHI (grant numbers 26293258, 19H01051, 20H03666 and 21H05044), JSID Fellowship Shiseido Research Grant, and research grants from the LEO Foundation, Takeda Science Foundation, Mochida Memorial Foundation for Medical and Pharmaceutical Research, and Keio Gijuku Academic Development Funds. The work was supported by the Intramural Research Programs of NIAMS (1 ZIA AR041159-09). Infrastructure of GC-MS to measure cholesterol-derived metabolites was supported by JST ERATO Suematsu Gas Biology Project (2010–2015, given to MS as the lead).

Data and materials availability:

Data for this study have been deposited to GEO (GSE175494 and GSE176039).

References and Notes:

1. Tait Wojno ED, Hunter CA, Stumhofer JS, The immunobiology of the interleukin-12 family: room for discovery. Immunity 50, 851–870 (2019). [PubMed: 30995503]
2. Chen Q, Ghilardi N, Wang H, Baker T, Xie MH, Gurney A, Grewal IS, de Sauvage FJ, Development of Th1-type immune responses requires the type I cytokine receptor TCCR. Nature 407, 916–920 (2000). [PubMed: 11057672]
3. Yoshida H, Hamano S, Senaldi G, Covey T, Faggioni R, Mu S, Xia M, Wakeham AC, Nishina H, Potter J, Saris CJ, Mak TW, WSX-1 is required for the initiation of Th1 responses and resistance to *L. major* infection. Immunity 15, 569–578 (2001). [PubMed: 11672539]
4. Villarino A, Hibbert L, Lieberman L, Wilson E, Mak T, Yoshida H, Kastelein RA, Saris C, Hunter CA, The IL-27R (WSX-1) is required to suppress T cell hyperactivity during infection. Immunity 19, 645–655 (2003). [PubMed: 14614852]
5. Hamano S, Himeno K, Miyazaki Y, Ishii K, Yamanaka A, Takeda A, Zhang M, Hisaeda H, Mak TW, Yoshimura A, Yoshida H, WSX-1 is required for resistance to *Trypanosoma cruzi* infection by regulation of proinflammatory cytokine production. Immunity 19, 657–667 (2003). [PubMed: 14614853]
6. Artis D, Villarino A, Silverman M, He W, Thornton EM, Mu S, Summer S, Covey TM, Huang E, Yoshida H, Koretzky G, Goldschmidt M, Wu GD, de Sauvage F, Miller HR, Saris CJ, Scott P, Hunter CA, The IL-27 receptor (WSX-1) is an inhibitor of innate and adaptive elements of type 2 immunity. J Immunol 173, 5626–5634 (2004). [PubMed: 15494513]
7. Artis D, Johnson LM, Joyce K, Saris C, Villarino A, Hunter CA, Scott P, Cutting edge: early IL-4 production governs the requirement for IL-27-WSX-1 signaling in the development of protective Th1 cytokine responses following Leishmania major infection. J Immunol 172, 4672–4675 (2004). [PubMed: 15067040]
8. Batten M, Li J, Yi S, Kljavin NM, Danilenko DM, Lucas S, Lee J, de Sauvage FJ, Ghilardi N, Interleukin 27 limits autoimmune encephalomyelitis by suppressing the development of interleukin 17-producing T cells. Nat Immunol 7, 929–936 (2006). [PubMed: 16906167]
9. Lucas S, Ghilardi N, Li J, de Sauvage FJ, IL-27 regulates IL-12 responsiveness of naive CD4+ T cells through Stat1-dependent and -independent mechanisms. Proc Natl Acad Sci U S A 100, 15047–15052 (2003). [PubMed: 14657353]
10. Diveu C, McGeachy MJ, Boniface K, Stumhofer JS, Sathe M, Joyce-Shaikh B, Chen Y, Tato CM, McClanahan TK, de Waal Malefyt R, Hunter CA, Cua DJ, Kastelein RA, IL-27 blocks RORc expression to inhibit lineage commitment of Th17 cells. J Immunol 182, 5748–5756 (2009). [PubMed: 19380822]

11. Hall AO, Beiting DP, Tato C, John B, Oldenhove G, Lombana CG, Pritchard GH, Silver JS, Bouladoux N, Stumhofer JS, Harris TH, Grainger J, Wojno ED, Wagage S, Roos DS, Scott P, Turka LA, Cherry S, Reiner SL, Cua D, Belkaid Y, Elloso MM, Hunter CA, The cytokines interleukin 27 and interferon-gamma promote distinct Treg cell populations required to limit infection-induced pathology. Immunity 37, 511–523 (2012). [PubMed: 22981537]
12. Awasthi A, Carrier Y, Peron JP, Bettelli E, Kamanaka M, Flavell RA, Kuchroo VK, Oukka M, Weiner HL, A dominant function for interleukin 27 in generating interleukin 10-producing anti-inflammatory T cells. Nat Immunol 8, 1380–1389 (2007). [PubMed: 17994022]
13. Fitzgerald DC, Zhang GX, El-Behi M, Fonseca-Kelly Z, Li H, Yu S, Saris CJ, Gran B, Ciric B, Rostami A, Suppression of autoimmune inflammation of the central nervous system by interleukin 10 secreted by interleukin 27-stimulated T cells. Nat Immunol 8, 1372–1379 (2007). [PubMed: 17994023]
14. Hirahara K, Ghoreschi K, Yang XP, Takahashi H, Laurence A, Vahedi G, Sciume G, Hall AO, Dupont CD, Francisco LM, Chen Q, Tanaka M, Kanno Y, Sun HW, Sharpe AH, Hunter CA, O'Shea JJ, Interleukin-27 priming of T cells controls IL-17 production in trans via induction of the ligand PD-L1. Immunity 36, 1017–1030 (2012). [PubMed: 22726954]
15. Chihara N, Madi A, Kondo T, Zhang H, Acharya N, Singer M, Nyman J, Marjanovic ND, Kowalczyk MS, Wang C, Kurtulus S, Law T, Etminan Y, Nevin J, Buckley CD, Burkett PR, Buenrostro JD, Rozenblatt-Rosen O, Anderson AC, Regev A, Kuchroo VK, Induction and transcriptional regulation of the co-inhibitory gene module in T cells. Nature 558, 454–459 (2018). [PubMed: 29899446]
16. Peters A, Pitcher LA, Sullivan JM, Mitsdoerffer M, Acton SE, Franz B, Wucherpfennig K, Turley S, Carroll MC, Sobel RA, Bettelli E, Kuchroo VK, Th17 cells induce ectopic lymphoid follicles in central nervous system tissue inflammation. Immunity 35, 986–996 (2011). [PubMed: 22177922]
17. Miyamoto Y, Uga H, Tanaka S, Kadowaki M, Ikeda M, Saegusa J, Morinobu A, Kumagai S, Kurata H, Podoplanin is an inflammatory protein upregulated in Th17 cells in SKG arthritic joints. Mol Immunol 54, 199–207 (2013). [PubMed: 23287598]
18. Kishi Y, Kondo T, Xiao S, Yosef N, Gaublomme J, Wu C, Wang C, Chihara N, Regev A, Joller N, Kuchroo VK, Protein C receptor (PROCR) is a negative regulator of Th17 pathogenicity. J Exp Med 213, 2489–2501 (2016). [PubMed: 27670590]
19. Blanc M, Hsieh WY, Robertson KA, Kropp KA, Forster T, Shui G, Lacaze P, Watterson S, Griffiths SJ, Spann NJ, Meljon A, Talbot S, Krishnan K, Covey DF, Wenk MR, Craigon M, Ruzsics Z, Haas J, Angulo A, Griffiths WJ, Glass CK, Wang Y, Ghazal P, The transcription factor STAT-1 couples macrophage synthesis of 25-hydroxycholesterol to the interferon antiviral response. Immunity 38, 106–118 (2013). [PubMed: 23273843]
20. Liu SY, Aliyari R, Chikere K, Li G, Marsden MD, Smith JK, Pernet O, Guo H, Nusbaum R, Zack JA, Freiberg AN, Su L, Lee B, Cheng G, Interferon-inducible cholesterol-25-hydroxylase broadly inhibits viral entry by production of 25-hydroxycholesterol. Immunity 38, 92–105 (2013). [PubMed: 23273844]
21. Iwata S, Mikami Y, Sun HW, Brooks SR, Jankovic D, Hirahara K, Onodera A, Shih HY, Kawabe T, Jiang K, Nakayama T, Sher A, O'Shea JJ, Davis FP, Kanno Y, The transcription factor T-bet limits amplification of type I IFN transcriptome and circuitry in T helper 1 cells. Immunity 46, 983–991 e984 (2017). [PubMed: 28623086]
22. Lund EG, Kerr TA, Sakai J, Li WP, Russell DW, cDNA cloning of mouse and human cholesterol 25-hydroxylases, polytopic membrane proteins that synthesize a potent oxysterol regulator of lipid metabolism. J Biol Chem 273, 34316–34327 (1998). [PubMed: 9852097]
23. Spann NJ, Glass CK, Sterols and oxysterols in immune cell function. Nat Immunol 14, 893–900 (2013). [PubMed: 23959186]
24. Brown MS, Goldstein JL, Cholesterol feedback: from Schoenheimer's bottle to Scap's MELADL. J Lipid Res 50 Suppl, S15–27 (2009). [PubMed: 18974038]
25. Goldstein JL, DeBose-Boyd RA, Brown MS, Protein sensors for membrane sterols. Cell 124, 35–46 (2006). [PubMed: 16413480]
26. Chen SS, Enhanced sterol synthesis in concanavalin A-stimulated lymphocytes: correlation with phospholipid synthesis and DNA synthesis. J Cell Physiol 100, 147–157 (1979). [PubMed: 468918]

27. Chen HW, Heiniger HJ, Kandutsch AA, Relationship between sterol synthesis and DNA synthesis in phytohemagglutinin-stimulated mouse lymphocytes. Proc Natl Acad Sci U S A 72, 1950–1954 (1975). [PubMed: 1057774]

28. Chakrabarti R, Engleman EG, Interrelationships between mevalonate metabolism and the mitogenic signaling pathway in T lymphocyte proliferation. J Biol Chem 266, 12216–12222 (1991). [PubMed: 1712015]

29. Takahashi H, Kouno M, Nagao K, Wada N, Hata T, Nishimoto S, Iwakura Y, Yoshimura A, Yamada T, Kuwana M, Fujii H, Koyasu S, Amagai M, Desmoglein 3-specific CD4+ T cells induce pemphigus vulgaris and interface dermatitis in mice. J Clin Invest 121, 3677–3688 (2011). [PubMed: 21821914]

30. Miyazaki Y, Shimanoe Y, Wang S, Yoshida H, Amelioration of delayed-type hypersensitivity responses by IL-27 administration. Biochem Biophys Res Commun 373, 397–402 (2008). [PubMed: 18572017]

31. Pereira JP, Kelly LM, Xu Y, Cyster JG, EBI2 mediates B cell segregation between the outer and centre follicle. Nature 460, 1122–1126 (2009). [PubMed: 19597478]

32. Hannedouche S, Zhang J, Yi T, Shen W, Nguyen D, Pereira JP, Guerini D, Baumgarten BU, Roggo S, Wen B, Knochenmuss R, Noel S, Gessier F, Kelly LM, Vanek M, Laurent S, Preuss I, Miault C, Christen I, Karuna R, Li W, Koo DI, Suply T, Schmedt C, Peters EC, Falchetto R, Katopodis A, Spanka C, Roy MO, Detheux M, Chen YA, Schultz PG, Cho CY, Seuwen K, Cyster JG, Sailer AW, Oxysterols direct immune cell migration via EBI2. Nature 475, 524–527 (2011). [PubMed: 21796212]

33. Cyster JG, Dang EV, Reboldi A, Yi T, 25-Hydroxycholesterols in innate and adaptive immunity. Nat Rev Immunol 14, 731–743 (2014). [PubMed: 25324126]

34. Simon A, Cholesterol metabolism and immunity. N Engl J Med 371, 1933–1935 (2014). [PubMed: 25390746]

35. Wang F, Beck-Garcia K, Zorzin C, Schamel WW, Davis MM, Inhibition of T cell receptor signaling by cholesterol sulfate, a naturally occurring derivative of membrane cholesterol. Nat Immunol 17, 844–850 (2016). [PubMed: 27213689]

36. Sakurai T, Uruno T, Sugiura Y, Tatsuguchi T, Yamamura K, Ushijima M, Hattori Y, Kukimoto-Niino M, Mishima-Tsumagari C, Watanabe M, Suematsu M, Fukui Y, Cholesterol sulfate is a DOCK2 inhibitor that mediates tissue-specific immune evasion in the eye. Sci Signal 11, (2018).

37. Park K, Scott AL, Cholesterol 25-hydroxylase production by dendritic cells and macrophages is regulated by type I interferons. J Leukoc Biol 88, 1081–1087 (2010). [PubMed: 20699362]

38. Shibata N, Carlin AF, Spann NJ, Saijo K, Morello CS, McDonald JG, Romanoski CE, Maurya MR, Kaikkonen MU, Lam MT, Crotti A, Reichart D, Fox JN, Quehenberger O, Raetz CR, Sullards MC, Murphy RC, Merrill AH Jr., Brown HA, Dennis EA, Fahy E, Subramaniam S, Cavener DR, Spector DH, Russell DW, Glass CK, 25-Hydroxycholesterol activates the integrated stress response to reprogram transcription and translation in macrophages. J Biol Chem 288, 35812–35823 (2013). [PubMed: 24189069]

39. Li C, Deng YQ, Wang S, Ma F, Aliyari R, Huang XY, Zhang NN, Watanabe M, Dong HL, Liu P, Li XF, Ye Q, Tian M, Hong S, Fan J, Zhao H, Li L, Vishlaghi N, Buth JE, Au C, Liu Y, Lu N, Du P, Qin FX, Zhang B, Gong D, Dai X, Sun R, Novitch BG, Xu Z, Qin CF, Cheng G, 25-Hydroxycholesterol protects host against zika virus infection and its associated microcephaly in a mouse model. Immunity 46, 446–456 (2017). [PubMed: 28314593]

40. Zhou QD, Chi X, Lee MS, Hsieh WY, Mkrtchyan JJ, Feng AC, He C, York AG, Bui VL, Kronenberger EB, Ferrari A, Xiao X, Daly AE, Tarling EJ, Damoiseaux R, Scumpia PO, Smale ST, Williams KJ, Tontonoz P, Bensinger SJ, Interferon-mediated reprogramming of membrane cholesterol to evade bacterial toxins. Nat Immunol 21, 746–755 (2020). [PubMed: 32514064]

41. Zang R, Case JB, Yutuc E, Ma X, Shen S, Gomez Castro MF, Liu Z, Zeng Q, Zhao H, Son J, Rothlauf PW, Kreutzberger AJB, Hou G, Zhang H, Bose S, Wang X, Vahey MD, Mani K, Griffiths WJ, Kirchhausen T, Fremont DH, Guo H, Diwan A, Wang Y, Diamond MS, Whelan SPJ, Ding S, Cholesterol 25-hydroxylase suppresses SARS-CoV-2 replication by blocking membrane fusion. Proc Natl Acad Sci U S A 117, 32105–32113 (2020). [PubMed: 33239446]

42. Bauman DR, Bitmansour AD, McDonald JG, Thompson BM, Liang G, Russell DW, 25-Hydroxycholesterol secreted by macrophages in response to Toll-like receptor activation

suppresses immunoglobulin A production. Proc Natl Acad Sci U S A 106, 16764–16769 (2009). [PubMed: 19805370]

43. Reboldi A, Dang EV, McDonald JG, Liang G, Russell DW, Cyster JG, Inflammation. 25-Hydroxycholesterol suppresses interleukin-1-driven inflammation downstream of type I interferon. Science 345, 679–684 (2014). [PubMed: 25104388]
44. Dang EV, McDonald JG, Russell DW, Cyster JG, Oxysterol restraint of cholesterol synthesis prevents AIM2 inflammasome activation. Cell 171, 1057–1071 e1011 (2017). [PubMed: 29033131]
45. Gold ES, Diercks AH, Podolsky I, Podyminogin RL, Askovich PS, Treuting PM, Aderem A, 25-Hydroxycholesterol acts as an amplifier of inflammatory signaling. Proc Natl Acad Sci U S A 111, 10666–10671 (2014). [PubMed: 24994901]
46. Vigne S, Chalmin F, Duc D, Clottu AS, Apetoh L, Lobaccaro JA, Christen I, Zhang J, Pot C, IL-27-induced type 1 regulatory T-cells produce oxysterols that constrain IL-10 production. Front Immunol 8, 1184 (2017). [PubMed: 28993775]
47. Bottemanne P, Paquot A, Ameraoui H, Guillemot-Legris O, Alhouayek M, Muccioli GG, 25-Hydroxycholesterol metabolism is altered by lung inflammation, and its local administration modulates lung inflammation in mice. FASEB J 35, e21514 (2021). [PubMed: 33734509]
48. Puleston DJ, Villa M, Pearce EL, Ancillary activity: beyond core metabolism in immune cells. Cell Metab 26, 131–141 (2017). [PubMed: 28683280]
49. Bensinger SJ, Bradley MN, Joseph SB, Zelcer N, Janssen EM, Hausner MA, Shih R, Parks JS, Edwards PA, Jamieson BD, Tontonoz P, LXR signaling couples sterol metabolism to proliferation in the acquired immune response. Cell 134, 97–111 (2008). [PubMed: 18614014]
50. Kidani Y, Elsaesser H, Hock MB, Vergnes L, Williams KJ, Argus JP, Marbois BN, Komisopoulou E, Wilson EB, Osborne TF, Graeber TG, Reue K, Brooks DG, Bensinger SJ, Sterol regulatory element-binding proteins are essential for the metabolic programming of effector T cells and adaptive immunity. Nat Immunol 14, 489–499 (2013). [PubMed: 23563690]
51. Yang W, Bai Y, Xiong Y, Zhang J, Chen S, Zheng X, Meng X, Li L, Wang J, Xu C, Yan C, Wang L, Chang CC, Chang TY, Zhang T, Zhou P, Song BL, Liu W, Sun SC, Liu X, Li BL, Xu C, Potentiating the antitumour response of CD8(+) T cells by modulating cholesterol metabolism. Nature 531, 651–655 (2016). [PubMed: 26982734]
52. Finotto S, Neurath MF, Glickman JN, Qin S, Lehr HA, Green FH, Ackerman K, Haley K, Galle PR, Szabo SJ, Drazen JM, De Sanctis GT, Glimcher LH, Development of spontaneous airway changes consistent with human asthma in mice lacking T-bet. Science 295, 336–338 (2002). [PubMed: 11786643]
53. Durbin JE, Hackenmiller R, Simon MC, Levy DE, Targeted disruption of the mouse Stat1 gene results in compromised innate immunity to viral disease. Cell 84, 443–450 (1996). [PubMed: 8608598]
54. Hata T, Nishifuji K, Shimoda K, Sasaki T, Yamada T, Nishikawa T, Koyasu S, Amagai M, Transgenic rescue of desmoglein 3 null mice with desmoglein 1 to develop a syngeneic mouse model for pemphigus vulgaris. J Dermatol Sci 63, 33–39 (2011). [PubMed: 21602032]

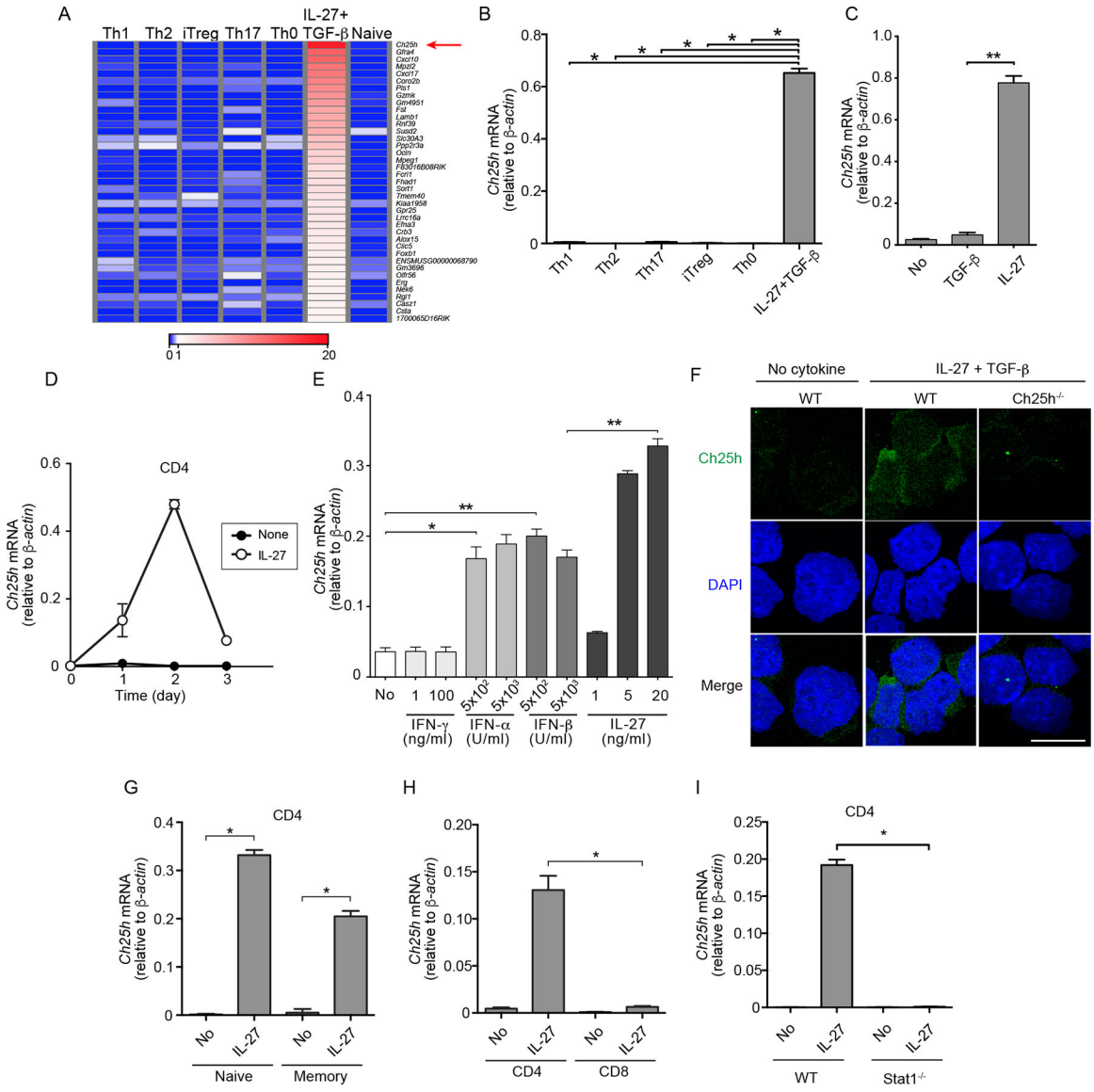

Figure 1. Ch25h is selectively induced in CD4$^+$ T cells stimulated with IL-27 and TGF-β.

(A) Heatmap of gene expression measured using mRNA-seq. Genes that are expressed in IL-27- and TGF-β-treated T cells, but not in other conditions, are selected and shown. Representative results from two independent experiments are shown. See also Fig. S1.

(B) *Ch25h* expression measured using RT-qPCR is shown relative to β-actin expression. Representative results from two independent experiments are shown. *$p < 0.0001$.

(C) *Ch25h* expression measured using RT-qPCR in naïve CD4$^+$ T cells treated with TGF-β or IL-27 along with anti-CD3 and anti-CD28 stimulation for 2 days. Representative results from two independent experiments are shown. **$p < 0.0001$.

(D) *Ch25h* expression measured using RT-qPCR daily over the course of 3 days in naïve CD4$^+$ T cells treated with or without IL-27 along with anti-CD3 and anti-CD28 stimulation. Representative results from two independent experiments are shown.

(E) *Ch25h* expression measured using RT-qPCR in naïve CD4$^+$ T cells treated with IFN-γ, IFN-α, IFN-β, or IL-27 in conjunction with anti-CD3 and anti-CD28 stimulation for 2 days.

Representative results from two independent experiments are shown. *$p < 0.0001$, **$p = 0.0002$.

(F) Ch25h protein expression detected using immunohistochemistry in wild-type and *Ch25h*$^{-/-}$ naïve CD4^{+} T cells treated with or without TGF-β and IL-27 along with anti-CD3 and anti-CD28 stimulation for 2 days. Ch25h staining is in green, and DAPI is in blue. Scale indicates 20 μm.

(G) *Ch25h* expression measured using RT-qPCR in CD4^{+}CD25^{-}CD62L^{hi}CD44^{lo} naïve or CD4^{+}CD25^{-}CD62L^{lo}CD44^{hi} memory T cells treated with or without IL-27 along with anti-CD3 and anti-CD28 antibody stimulation for 2 days. Representative results from four independent experiments are shown. *$p < 0.0001$.

(H) *Ch25h* expression measured using RT-qPCR in CD4^{+} or CD8^{+} naïve T cells treated with or without IL-27 along with anti-CD3 and anti-CD28 antibody stimulation for 2 days. Representative results from three independent experiments are shown. *$p < 0.0001$.

(I) *Ch25h* expression measured using RT-qPCR in wild-type and *Stat1*$^{-/-}$ naïve CD4^{+} T cells treated with or without IL-27 along with anti-CD3 and anti-CD28 antibody stimulation. Representative results from three independent experiments are shown. *$p < 0.0001$.

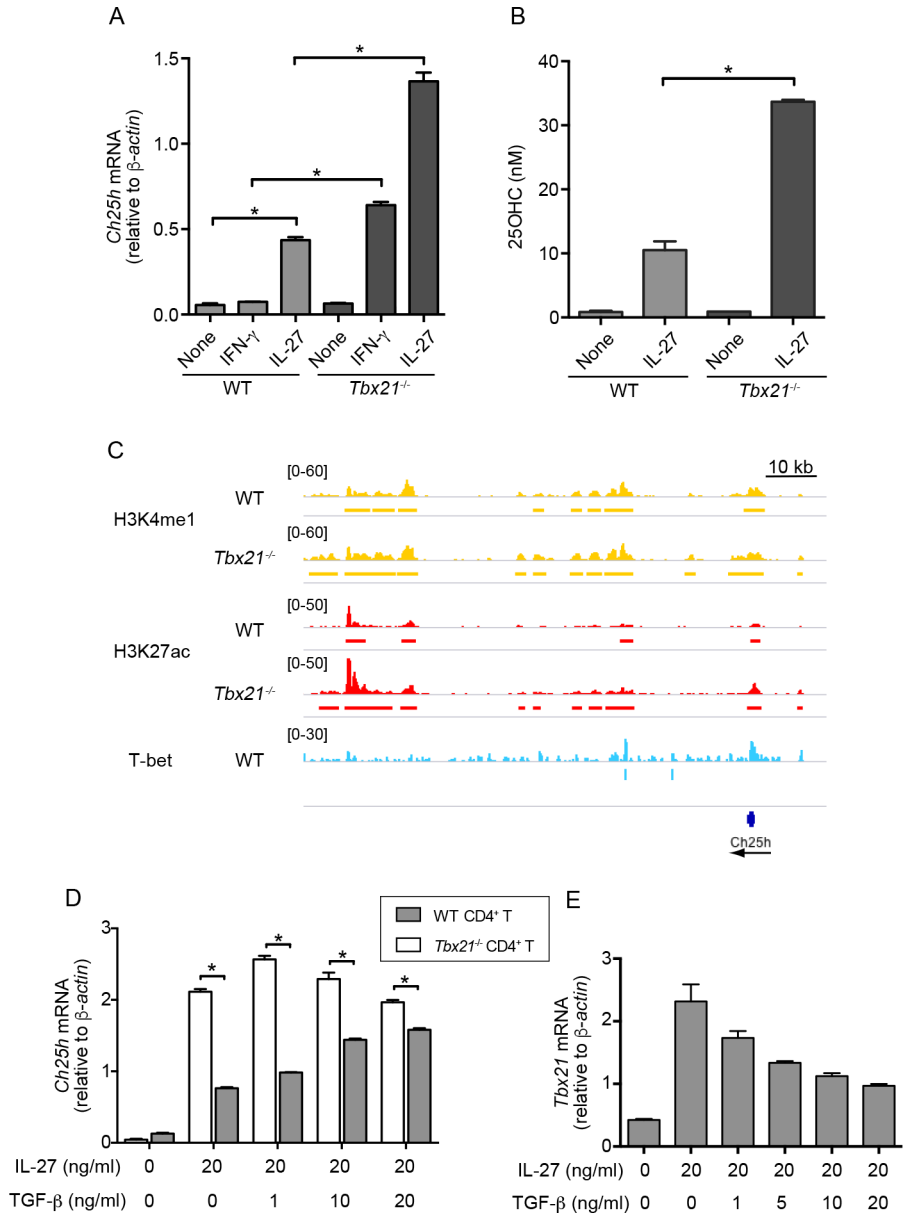

Figure 2. T-bet negatively regulates *Ch25h* expression in CD4$^+$ T cells.

(A) *Ch25h* expression measured using RT-qPCR in wild-type and *Tbx21*$^{-/-}$ naïve CD4$^+$ T cells treated with IFN-γ or IL-27 along with anti-CD3 and anti-CD28 stimulation for 2 days. Representative results from two independent experiments are shown. *$p < 0.0001$.

(B) Amounts of 25OHC secreted in the culture supernatant measured using GC-MS following stimulation of wild-type and *Tbx21*$^{-/-}$ naïve CD4$^+$ T cells with IL-27 for 3 days. Representative results from four independent experiments are shown. *$p < 0.0001$.

(C) Genome track views of the extended *Ch25h* locus showing the deposition of H3K4me1 (yellow), H3K27ac (red), and T-bet (blue) in wild-type and *Tbx21*$^{-/-}$ naïve CD4$^+$ T cells. ChIP-seq data (GSE96724) reported previously (21) were re-analyzed, and peaks with significance (default *p*-value threshold of 1E^{-5}) are underlined.

(D) *Ch25h* expression measured using RT-qPCR in wild-type (gray) and *Tbx21*$^{-/-}$ (white) naïve CD4^{+} T cells treated with various combinations of IL-27 and TGF-β along with anti-CD3 and anti-CD28 stimulation for 2 days. Representative results from two independent experiments are shown. *$p < 0.001$.

(E) *Tbx21* expression measured using RT-qPCR in naïve CD4^{+} T cells treated with various combinations of IL-27 and TGF-β along with anti-CD3 and anti-CD28 stimulation for 2 days. Representative results from three independent experiments are shown.

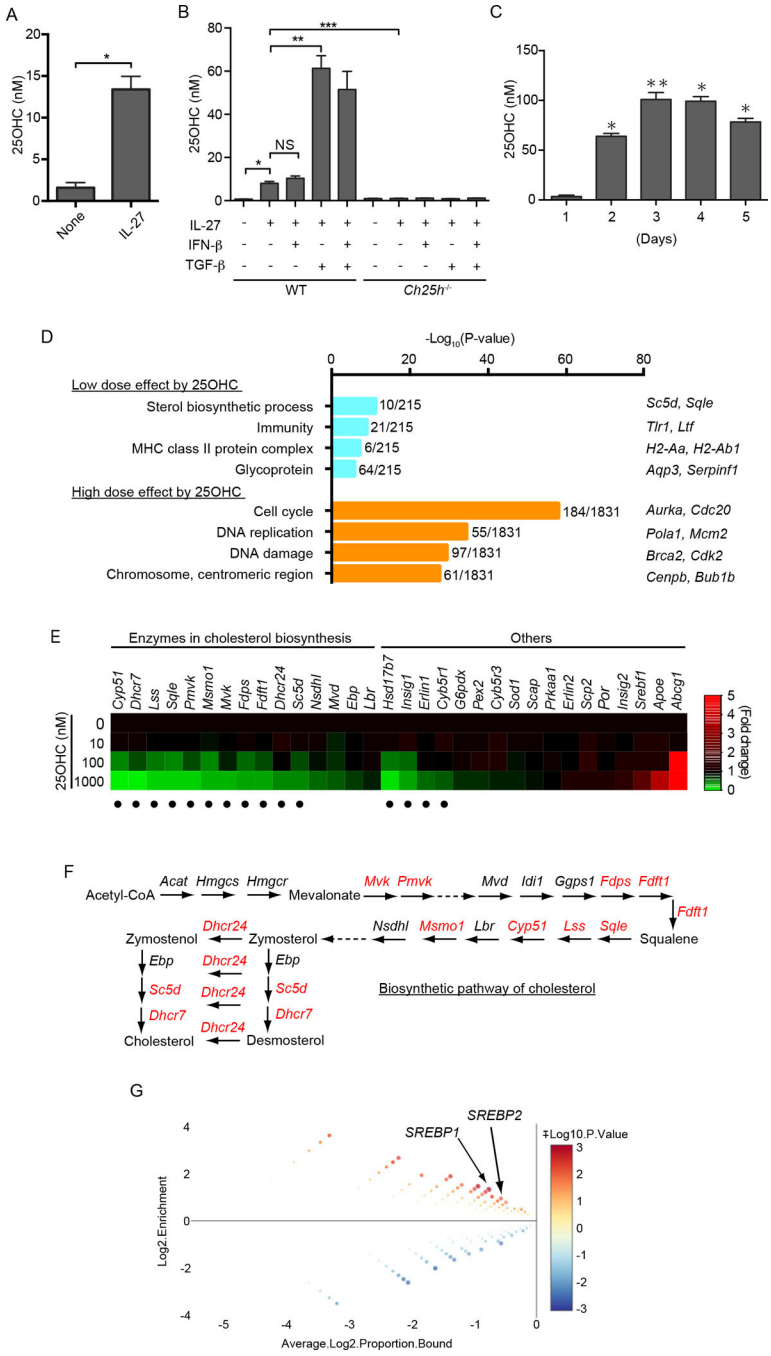

Figure 3. Ch25h-expressing CD4$^+$ T cells produce 25OHC that down-regulates gene expression of cholesterol biosynthetic enzymes

(A) Amount of 25OHC secreted in the culture supernatant measured using gas chromatography-mass spectrometry (GC-MS) following stimulation of naïve CD4$^+$ T cells by anti-CD3 and anti-CD28 antibodies and the indicated cytokines for 3 days. Representative results from three independent experiments are shown. *p = 0.002.

(B) Amount of 25OHC secreted in the culture supernatant measured using GC-MS following stimulation of wild-type and *Ch25h*$^{-/-}$ naïve CD4$^+$ T cells with various combinations of IL-27, IFN-β and TGF-β in the presence of anti-CD3 and anti-CD28

antibodies for 3 days. Representative results from three independent experiments are shown. *$p = 0.0002$, **$p = 0.0001$, ***$p = 0.001$.

(C) Amount of 25OHC secreted in the culture supernatant measured using GC-MS daily during the course of naïve $CD4^+$ T cell stimulation with coated anti-CD3 and anti-CD28 antibodies and IL-27 and TGF-β. Representative results from three independent experiments are shown. Statistical significance was calculated in comparison with the value on day 1. *$p < 0.0001$, **$p = 0.0002$.

(D) Differentially expressed genes (DEGs) after 25OHC treatment are depicted and were subjected to pathway analysis using DAVID and mRNA-seq data. A total of 215 DEGs were identified by comparing 10 nM and 100 nM 25OHC conditions, and 1831 DEGs were identified by comparing 100 and 1000 nM 25OHC conditions. The top four biological pathways identified are shown for low (blue) and high (orange) dose effects. The number of genes involved in the corresponding pathways and names of representative genes is also included. See also Tables S2 and S3.

(E) Gene expression heatmap showing genes assigned to the sterol biosynthetic process identified in Figure 3D. Cells were harvested following 24 h of 25OHC treatment and subjected to mRNA-seq analysis. Genes showing more than a two-fold decrease in treated cells compared to untreated cells are marked with black dots. See also Fig. S3 and Table S4.

(F) An outline of the cholesterol biosynthetic pathway. Gene symbols of representative enzymes and names of metabolic intermediates are shown. Gene symbols that showed decreased expression following 25OHC treatment are colored in red.

(G) Transcription factor enrichment plot. Transcription factor-binding DNA motifs enriched in 25OHC-mediated downregulated genes among genes annotated as cholesterol biosynthesis were plotted by CiiiDER. The $-\log_{10}$ *p*-values for SREBP1 and SREBP2 are 3.02 and 2.14, respectively.

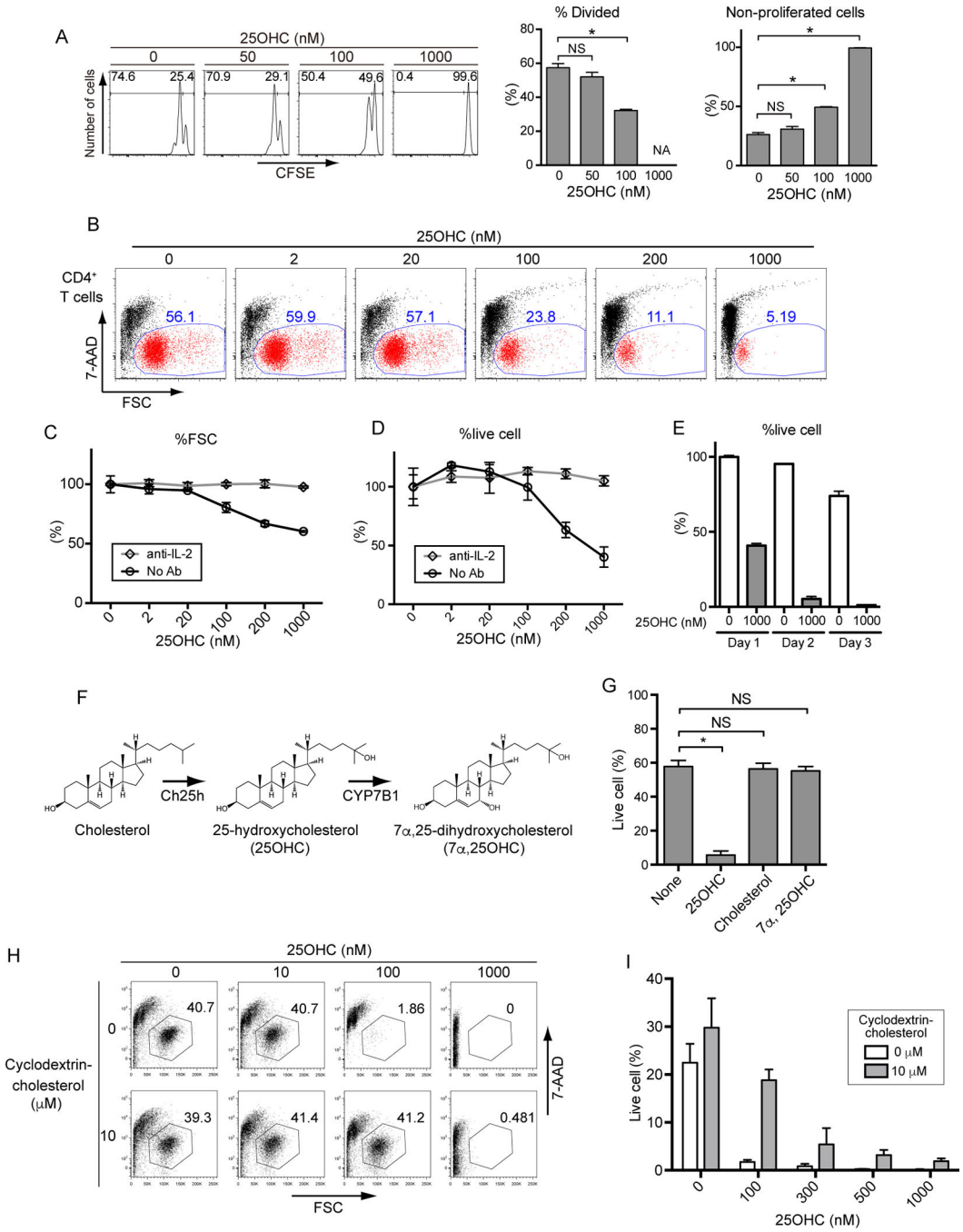

Figure 4. 25OHC impairs cell proliferation and induces cholesterol-deprived cell death.

(A) CFSE dilution assay of naïve CD4$^+$ T cells after anti-CD3 and anti-CD28 stimulation with various concentrations of 25OHC. Proliferation as quantified by %Divided calculated by FlowJo along with the proportion of non-divided cells are shown in the graphs. Representative results from two independent experiments are shown. *$p < 0.05$. NA, not applicable. NS, not significant.

(B) Flow cytometric analysis to detect live cells (red dots) following anti-CD3 and anti-CD28 stimulation of naïve CD4$^+$ T cells for 3 days with various concentrations of

25OHC in the absence of additional cytokines. Dead cells are quantitated by staining with 7-aminoactinomycin D. Numbers indicate the proportions of live cells. Representative results from four independent experiments are shown.

(C) Dose-dependent effects of 25OHC on forward scatter profile comparing control and anti-IL-2 antibody-supplemented conditions in conjunction with T-cell receptor stimulation, as shown in Figure 4B. Values of untreated cells were set as 100%.

(D) 25OHC-mediated dose-dependent changes in live cells in the experiment similar to (C). Values for untreated cells were set as 100%.

(E) 25OHC-mediated changes in live cells over time. Values for untreated cells at day 1 were set as 100%. Representative results from two independent experiments are shown.

(F) Cholesterol metabolism pathway.

(G) Fractions of live cells treated with cholesterol, 25OHC, and 7α,25OHC are shown. Representative results from three independent experiments are shown. *$p < 0.0001$.

(H) Flow cytometric analyses to detect live cells treated with various concentrations of 25OHC in combination with or without cyclodextrin–cholesterol. Representative results from three independent experiments are shown.

(I) The proportion of live cells treated with 25OHC in combination with or without cyclodextrin–cholesterol is shown. Representative results from two independent experiments are shown.

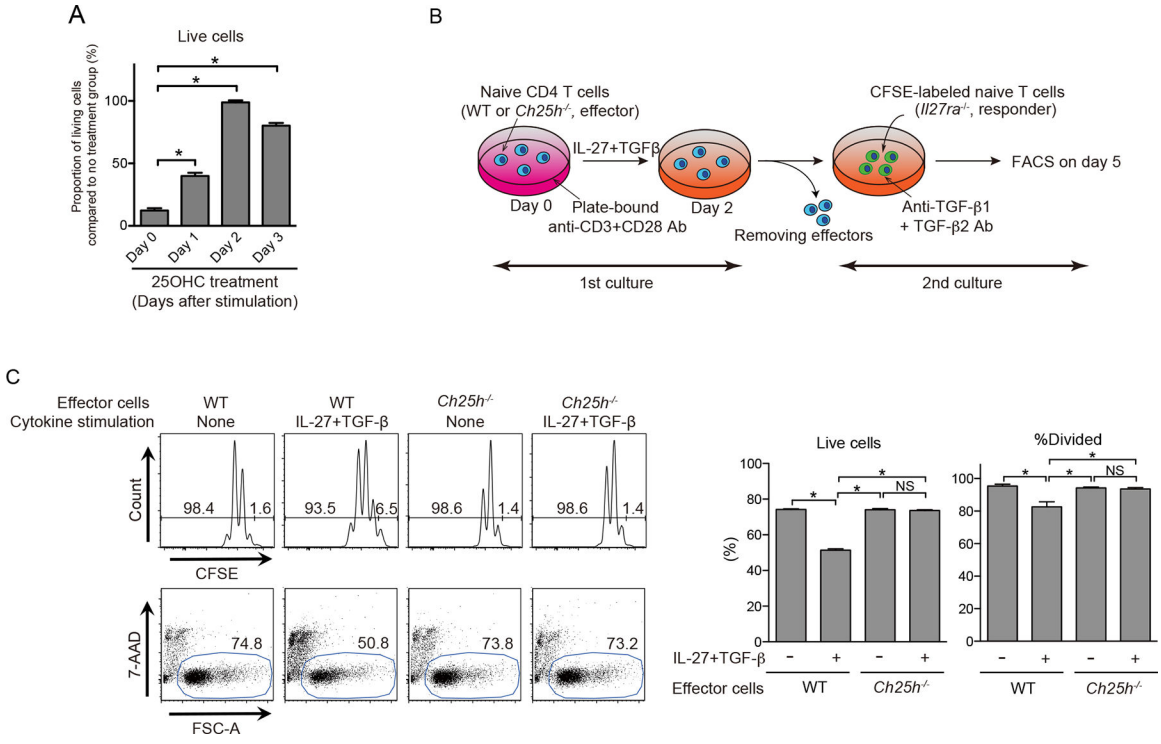

Figure 5. Ch25h-expressing CD4$^+$ T cells impair viability of bystander T cells at early stage of TCR activation in a paracrine manner

(A) CD4$^+$ T cells were stimulated with anti-CD3 and CD28 antibodies at day 0 and cultured with 200 nM 25OHC at the time points indicated. Three days later, the percent of living cells was analyzed. 25OHC non-treated CD4$^+$ T cells were simultaneously analyzed. The ratios of living cells in 25OHC-treated cells as a percent of non-treated cells are depicted. Representative results from two independent experiments are shown. *$p < 0.05$.

(B) Schematic overview for experiments in Fig. 5C.

(C) In FACS plots, proportion of 7-AAD$^-$ living cells (lower panels) and dilution of CFSE-labeled responder cells (upper panels) were analyzed. In histograms, % divided responder cells were calculated by FlowJo. Representative results from three independent experiments are shown. *$p < 0.05$. NS, not significant.

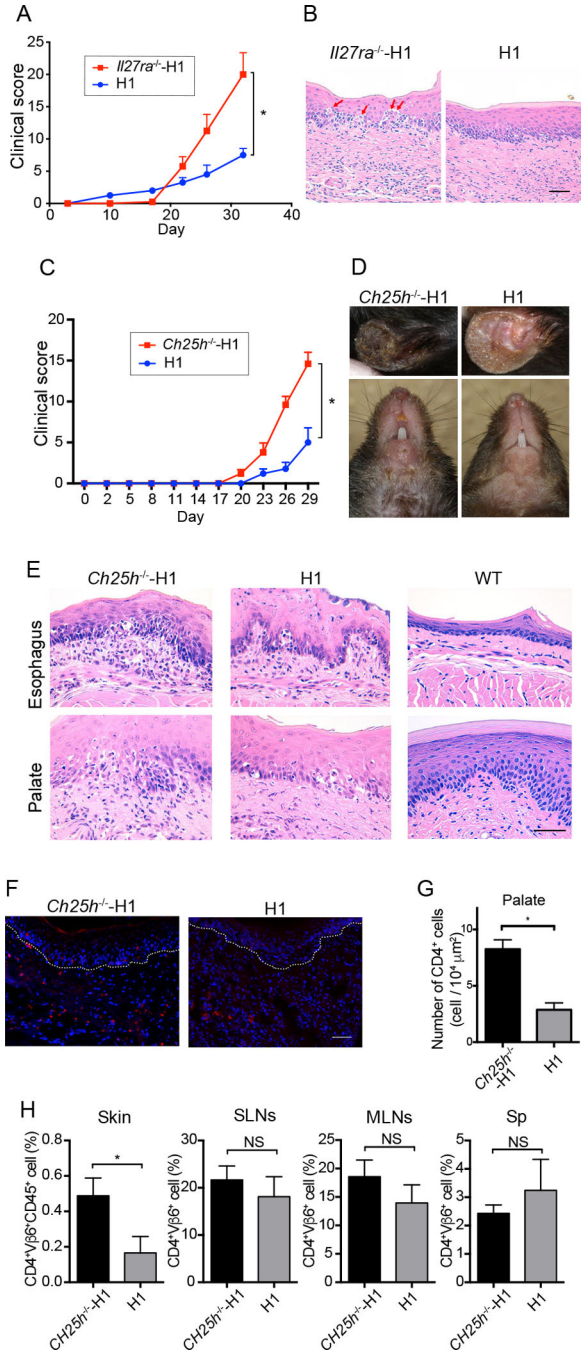

Figure 6. *Ch25h* expressed in T cells constrains tissue inflammation in experimental autoimmune dermatitis.

(A) Desmoglein 3 (Dsg3)-specific naïve $CD4^+$ T cells ($TCRV\beta6^+CD25^-CD62L^{hi}CD44^{lo}$) were isolated from H1 mice and *Il27ra*$^{-/-}$-H1 mice and transferred to *Rag2*$^{-/-}$ mice (n = 4 in each group). Clinical scores were measured following the course of induced dermatitis. Representative results from three independent experiments are shown. *$p < 0.05$ (two-way ANOVA).

(B) Histopathology (hematoxylin and eosin staining) of the palate from two groups of treated mice on day 35. Red arrows indicate keratinocyte degeneration. Bar indicates 100 μm.

(C) Dsg3-specific naïve $CD4^+$ T cells were isolated from H1 mice and *Ch25h*$^{-/-}$-H1 mice and transferred to *Rag2*$^{-/-}$ mice to induce skin inflammation (n = 5 in each group). Clinical scores were measured following the course of induced dermatitis. Representative results from three independent experiments are shown. $*p = 0.002$ (two-way ANOVA).

(D) Skin inflammation observed in *Rag2*$^{-/-}$ recipient mice transferred with Dsg3-specific naïve $CD4^+$ T cells derived from H1 (right panels) and *Ch25h*$^{-/-}$-H1 (left panels) donors.

(E) Histopathology of the palate and esophagus of *Rag2*$^{-/-}$ recipient mice receiving wild-type (middle) or *Ch25h*$^{-/-}$ (left) H1 $CD4^+$ T cells. The palate and esophagus of wild-type mice are also shown (right). The scale bar indicates 50 μm.

(F) Immunofluorescence staining of the palate with TCRVβ (red) and DAPI (blue) of *Rag2*$^{-/-}$ recipient mice receiving wild-type (right) or *Ch25h*$^{-/-}$ (left) H1 $CD4^+$ T cells. The scale bar indicates 50 μm.

(G) Numbers of $CD4^+$ T cells in the palate of *Rag2*$^{-/-}$ recipient mice receiving wild-type or *Ch25h*$^{-/-}$ H1 $CD4^+$ T cells. Cells gated by a square 100 μm on a side were counted using the images in (F). $*p = 0.001$.

(H) Flow cytometric analysis of Dsg3-specific $CD4^+$ T cells. Cells in the skin, skin-draining LNs (SLNs), mesenteric LNs (MLNs), and spleen (Sp) were compared between mice transferred with wild-type or *Ch25h*$^{-/-}$ H1 $CD4^+$ T cells. $*p = 0.045$.

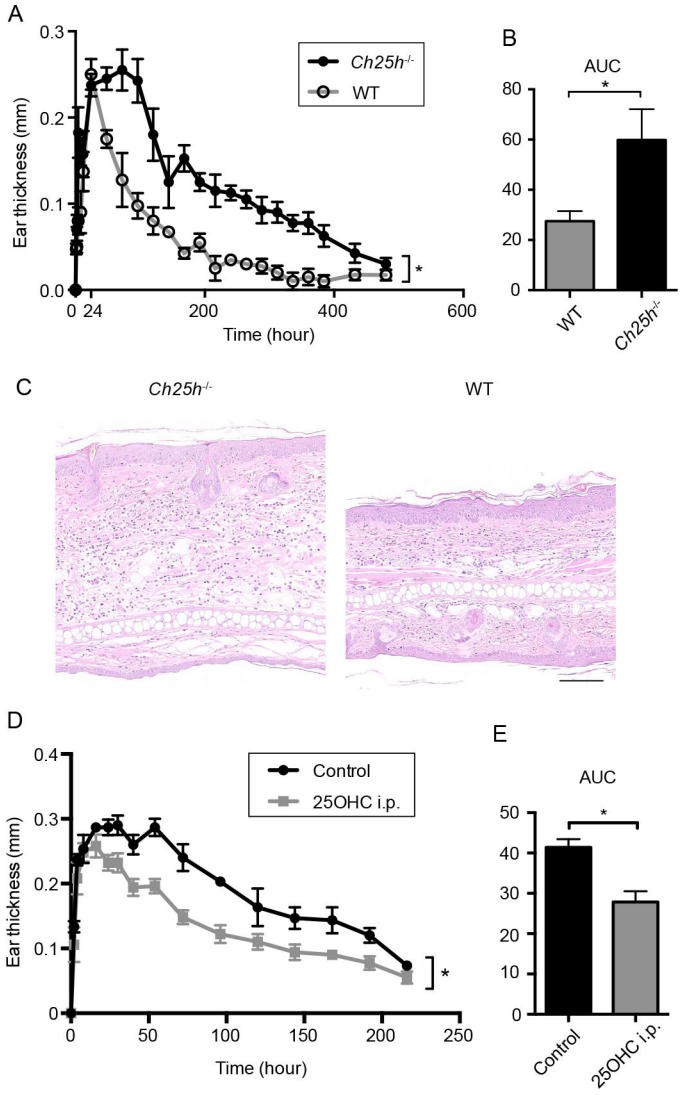

Figure 7. Absence of Ch25h exacerbates skin contact hypersensitivity.

(A - C) Contact hypersensitivity was elicited by DNFB sensitization and reapplication to ear skin in WT (n = 4) and *Ch25h*$^{-/-}$ mice (n = 4). Ear skin thickness was measured (A) and calculated as area under the curve (AUC) (B). Histopathology at 72 hours after elicitation is shown (C). Representative results from two independent experiments are shown. Bar indicates 100 μm.

(D – E) DNFB-induced contact hypersensitivity was elicited after 25OHC (n = 4) or vehicle (n = 3) i.p. injection once a day for five days after sensitization. Ear skin thickness was measured (D) and area under the curve (AUC) was shown (E). *$p < 0.05$. Similar results were obtained from two independent experiments.